NASA CR-135120
CMU-NASA-3Ti

INVESTIGATION OF THE FRACTURE MECHANISM IN Ti-5Al-2.5Sn AT CRYOGENIC TEMPERATURES

by R. H. Van Stone,* J. R. Low, Jr.,* and J. L. Shannon, Jr.**

CARNEGIE-MELLON UNIVERSITY

prepared for

NATIONAL AERONAUTICS AND SPACE ADMINISTRATION

NASA Lewis Research Center
Contract NGR-39-087-047

FINAL REPORT
April 1977

*Department of Metallurgy and Materials Science, Carnegie-Mellon University, Pittsburgh, Pennsylvania 15213

**National Aeronautics & Space Administration, Lewis Research Center, Cleveland, Ohio 41135

1. Report No.	2. Government Accession No.	3. Recipient's Catalog No.
NASA CR 135120		

4. Title and Subtitle	5. Report Date
Investigation of the Fracture Mechanism in Ti-5Al-2.5Sn at Cryogenic Temperatures	April 1977 - FINAL REPORT
	6. Performing Organization Code

7. Author(s)	8. Performing Organization Report No.
R. H. Van Stone, J. R. Low, Jr., and J. L. Shannon, Jr.	NASA - 3 Ti
	10. Work Unit No.

9. Performing Organization Name and Address	11. Contract or Grant No.
Carnegie-Mellon University Department of Metallurgy and Materials Science 5000 Forbes Avenue Pittsburgh, Pennsylvania 15213	NGR-39-087-047
	13. Type of Report and Period Covered
12. Sponsoring Agency Name and Address	Grant
National Aeronautics and Space Administration Washington, D. C.	14. Sponsoring Agency Code

15. Supplementary Notes

Project Manager, William D. Klopp, Head, Materials Development Section, NASA Lewis Resesrch Center, Cleveland, Ohio

16. Abstract

The influence of microstructure on the fracture mechanism and plane-strain fracture toughness (K_{Ic}) of Ti-5Al-2.5Sn was studied through the use of fractography and metallographic sectioning techniques. One-inch thick plates of extra low interstitial (ELI) and normal interstitial Ti-5Al-2.5Sn were mill annealed at 815°C (1500°F) followed by either air or furnace cooling. These variations in composition and cooling rate resulted in differences in the volume fraction and internal structure of the iron-stabilized β phase, and in the crystallographic texture and ordering of the α matrix. The tensile properties and K_{Ic} of these plates were determined at 20°K (-423°F), 77°K (-320°F), and 295°K (72°F). The air-cooled ELI plate was the toughest material evaluated. K_{Ic} of the furnace-cooled ELI plate was about 25 percent below that of the air-cooled ELI material. Cooling rate from the annealing temperature had no influence on the toughness of the normal interstitial plates both of which had a K_{Ic} approximately half that of the air-cooled ELI plate. The 20°K fracture toughness of the normal interstitial plates did not vary significantly with specimen orientation. The LS toughness of both ELI plates was approximately 20 percent greater than the LT toughness. Fractography showed that a large portion of the fracture surfaces were covered with elongated dimples commonly called "flutes". Metallographic sections of specimens deformed at 77°K showed that these features form at the intersections of slip bands or deformation twins with grain or twin boundaries. Ordering and higher interstitial levels increase the local strain in slip bands resulting in void nucleation at lower macroscopic strains and lower K_{Ic} values.

17. Key Words (Suggested by Author(s))	18. Distribution Statement
Ti-5Al-2.5Sn, Cryogenic Temperatures, Plane Strain Fracture Toughness (K_{Ic}), Microstructure, Crystallographic Texture, Fracture, Fractography, Dimpled Rupture, Slip Bands, Deformation Twins	Unclassified - unlimited

19. Security Classif. (of this report)	20. Security Classif. (of this page)	21. No. of Pages	22. Price*
Unclassified	Unclassified	112	

* For sale by the National Technical Information Service, Springfield, Virginia 22151

INTRODUCTION AND SUMMARY

This is the final report of an investigation on the influence of microstructure on the fracture mechanism and fracture toughness of Ti-5Al-2.5Sn at cryogenic temperatures. The report is divided into two parts.

Part I describes the microstructural portion of the investigation which relied heavily on fractography and metallographic sectioning techniques. It was shown that the fracture process in Ti-5Al-2.5Sn occurs by nucleation, growth, and coalescence of voids which nucleate at the intersection of highly localized shear bands with crystallographic boundaries. Decreased interstitial content and rapid cooling from the annealing temperature so as to avoid ordering decreases the strain localization, reduces the rate of void nucleation, and improves fracture toughness.

Part II describes the tensile and plane-strain fracture toughness (K_{Ic}) properties of the Ti-5Al-2.5Sn plates and the techniques used to measure those properties at temperatures as low as 20°K (-423°F). The variation in strength level, work-hardening, and K_{Ic} is given as a function of temperature, interstitial content, cooling rate from the annealing temperature, and specimen orientation. It was shown that K_{Ic} increases with increasing temperature, decreasing interstitial content, and more rapid cooling rates from the annealing temperature.

PART I

THE FRACTURE MECHANISM OF Ti-5Al-2.5Sn AT CRYOGENIC TEMPERATURES

INTRODUCTION

Since the early 1970's, there has been a substantial research and development effort to exploit new sources of energy. One popular approach is the liquid hydrogen economy where energy is generated by nuclear or solar energy, converted into liquid hydrogen, and transported to an energy consuming market. One of the most difficult technological problems in this approach is a safe way to transport liquid hydrogen. One of the alloys commonly used to construct liquid hydrogen storage tanks in American spacecraft has been Ti-5Al-2.5Sn. This alloy was chosen due to its high strength-to-density ratio and its excellent combination of smooth and notched tensile properties.[1] Investigators have studied the microstructure,[2,3] deformation modes,[2] and mechanical properties[1,4,5] of Ti-5Al-2.5Sn, but virtually no attention has been paid to direct observations of the influence of microstructure on the fracture mechanism. The purpose of this investigation is to identify those microstructural features which participate in the fracture process of Ti-5Al-2.5Sn at cryogenic temperatures. It is hoped that these results can be used to make suggestions on how to improve the fracture toughness of this alloy without having a corresponding reduction in strength level.

LITERATURE REVIEW

Ti-5Al-2.5Sn is considered to be an α titanium alloy which has a hexagonal close packed crystal structure. This alloy is based largely on the titanium-aluminum phase diagram. Increases in aluminum concentration stabilize the α phase and result in the precipitation of the long-range ordered α_2 phase.[6] This phase has a hexagonal DO_{19} crystal structure

and has a range of compositions close to Ti_3Al. Blackburn[6] and Namboodhiri, et al.[7] used thin foil transmission electron microscopy (TEM) to determine the solvus line between the α and $\alpha+\alpha_2$ phase fields. At 500°C in Ti-Al alloys, this solvus line is at approximately 6 weight percent aluminum. If the tin in Ti-5Al-2.5Sn was replaced by aluminum on an atom basis, this alloy would be a titanium - 5.7 weight percent aluminum alloy. The titanium-tin phase diagram also has an ordered phase with DO_{19} crystal structure and with a composition close to Ti_3Sn.[8] Williams and Blackburn[9] have shown that substituting tin for aluminum on an atom basis expands the $\alpha+\alpha_2$ phase field. Thus it seems quite likely that α_2 could exist in Ti-5Al-2.5Sn alloys with a composition of Ti_3 (Al, Sn). Several investigations have used thin foil TEM to try to find α_2 in both annealed[3] and aged[2] Ti-5Al-2.5Sn, but no superlattice reflections have ever been observed.

Deformation of α titanium occurs by both slip and twinning.[10] Increases in oxygen content, increases in aluminum content, and reductions in deformation temperature cause the dislocation arrangements to go from a tangled, wavy morphology to planar, coarse slip. Once the slip becomes planar, further increases in solute or lowering of deformation temperature causes the spacing between slip bands to increase. Precipitation of α_2 also increases slip band spacing. Paton, Baggerly, and Williams[11] showed that increases in aluminum concentration, α_2 precipitation, and decreases in test temperature increase the critical resolved shear stress for prism, basal, and c+a slip. Corresponding increases in polycrystalline yield strength have also been observed. Twinning has been studied far less extensively than deformation by slip. Five twin systems are known to operate below room temperature.[10] Increased interstitial[10,12]

and aluminum contents[11] decrease the twin volume fraction while decreasing deformation temperatures below room temperature increase the frequency of twinning. The influence of grain size on twin volume fraction in α titanium has not been established.

Several investigations determined the mechanical properties of Ti-5Al-2.5Sn sheet material below room temperature. These investigations preceded the development of linear elastic fracture mechanics, so notched tensile specimens were used to assess toughness. Christian, et al.[4] tested annealed Ti-5Al-2.5Sn at 20°K and 77°K and showed that increased oxygen content resulted in higher tensile strength, lower tensile ductility, and a lower notched-to-unnotched strength ratio. Shannon and Brown[1] investigated the effect of cooling rate from an 815°C annealing treatment on smooth and notched tensile properties of extra low interstitial (ELI) Ti-5Al-2.5Sn sheet. At 20°K, air-cooled and furnace-cooled sheet has essentially identical smooth tensile properties, but the notched strength of the furnace-cooled sheet was about 25 percent below that of the air-cooled material. These investigations attributed the embrittlement to α_2 precipitation; however, no attempt was made to experimentally observe α_2. Curtis, Boyer, and Williams[2] showed that step-aging of Ti-5Al-2.5Sn plate at 593°C and 500°C did not change tensile strength but caused substantial decreases in room temperature toughness measured with precracked specimens. Thin foil TEM of the aged material failed to reveal any α_2 superlattice reflections. Although the decrease in toughness associated with furnace-cooling or aging Ti-5Al-2.5Sn could not be blamed on precipitation of α_2, embrittlement of Ti-8Al-1V-1Mo,[13] Ti-6Al-2Sn-4Zr-2Mo,[14] and Ti-5Al-5Sn-5Zr[2] has been attributed to α_2 precipitation. Reports that post-annealing heat treatment cycles have no

effect on the toughness of Ti-5Al-2.5Sn were based on tensile ductility data which is a very poor measure of toughness in titanium alloys.[15]

There have been very few investigations of the fracture mechanism of α titanium alloys particularly at cryogenic temperature. Williams, et al.[16] showed that the fracture mode of Ti-5Al-2.5Sn is dimpled rupture at room temperature. Beevers and Edmonds[17] showed that a titanium - 0.25 percent oxygen alloy failed at 77°K with seven micron equiaxed dimples and relatively flat elongated features approximately 80 microns long. Amateau and co-workers[18,19] studied the fracture mechanism in α titanium with 0.5 mm grain sizes. From observations on the prepolished specimens, they reported cracking by cleavage, cracking along twin boundaries and grain boundaries. These reports of cleavage were not substantiated by fractography.

SCOPE OF THIS INVESTIGATION

Based on previous work on Ti-5Al-2.5Sn alloys, the most reasonable approach to obtain material with a wide range of toughness would be to study Ti-5Al-2.5Sn with different interstitial contents and with different cooling rates from the annealing temperatures. In this investigation, the fracture mechanism of Ti-5Al-2.5Sn was studied in commercially produced ELI and normal interstitial grade plates. Sections of plate of both compositions were air-cooled or furnace-cooled after annealing. The microstructure of the plates was characterized and tensile properties and plane strain fracture toughness (K_{Ic}) of the plates were measured at 295°K, 77°K, and 20°K. The fracture mechanism was studied using fractography and metallographic sectioning techniques. The observations of sectioned specimens permits direct identification of

microstructural features which participate in the fracture process. Specimens were strained to several levels up to and including that required for fracture and sectioned so as to observe regions deformed under the constraint of surrounding material.

MATERIAL AND MICROSTRUCTURE

One inch thick Ti-5Al-2.5Sn plate of ELI and normal interstitial grade were commercially produced and annealed. The air-cooled and furnace-cooled plates of the same grade were produced from the same heat to avoid minor variations in composition. The compositional specification, heat analyses, and check analyses are given in Table I. In the normal interstitial plates, the oxygen content is approximately three times greater and the iron level about two times larger than those of the ELI alloy. The non-interstitial element iron varies with interstitial content and may significantly influence the structure and properties of the plates due to the strong β phase stabilization effect of iron.[20] Throughout this paper, the designation of alloy purity will be the interstitial content even though the iron levels also change significantly. Comparison of the oxygen contents of the air-cooled and furnace-cooled plates of each grade shows that the slower cooling rates resulted in no interstitial contamination.

The plates were annealed in the α phase field at 815°C (1500°F). The furnace-cooling rate is approximately 15C°/hour while the initial air-cooling rate is approximately 4500C°/hour. These rates are different by a factor of about 300, so there is a real possibility that the more slowly cooled plates remain at relatively high temperatures for enough time so that ordering may occur.

TABLE I

CHEMICAL ANALYSES OF Ti - 5 Al - 2.5 Sn ALLOYS
(Weight Percent)

	Al	Sn	Fe	Mn	O	C	N	H
Normal Int. Specification	4.0/6.0	2.0/3.0	0.50 Max	0.30 Max	0.20 Max	0.15 Max	0.07 Max	0.003/0.020
Normal Int. Heat Analysis	5.1	2.5	0.28	0.006	0.16	0.024	0.023	0.009
Normal Int., AC* Check Analysis	5.22	2.47	0.300	0.002	0.164	0.0140	0.0163	0.0072
Normal Int., FC† Check Analysis	5.24	2.47	0.270	0.002	0.169	0.0120	0.0172	0.0042
ELI Specification	4.7/5.6	2.0/3.0	0.1/0.2	--	0.12 Max	0.08 Max	0.05 Max	0.0125 Max
ELI Heat Analysis	5.0	2.6	0.16	0.006	0.086	0.023	0.010	0.006
ELI, AC * Check Analysis	5.09	2.44	0.140	0.002	0.054	0.0057	0.0098	0.0056
ELI, FC † Check Analysis	5.10	2.47	0.145	0.002	0.052	0.0041	0.0098	0.0050
Maximum Error in Check Analysis	0.200	0.150	0.010	0.0005	0.010	0.0010	0.0010	0.0010

* Air Cooled
† Furnace Cooled

The microstructure of these plates was examined using optical metallography, microprobe analysis, and thin foil TEM. Specimens for optical metallography were mechanically polished and etched in a solution of 3 percent hydrofluoric acid and 9 percent nitric acid in methanol which was held at $0^{\circ}C$ in an ice-water bath. Thin foils for TEM were prepared using the electrolyte described by Blackburn and Williams[21] in a jet polishing unit.

Figure 1 shows an optical micrograph of the furnace-cooled normal interstitial plate. The grains in all specimens were equiaxed indicating a well annealed structure. The intercept grain sizes for the four alloys are given in Table II. The grain sizes of the plates are approximately 40 microns except for the furnace-cooled ELI alloy which has a 58 micron grain size.

Figure 1 also shows a dispersed phase approximately 5 microns in diameter. This phase was observed in all the alloys. It had a lower volume fraction and was approximately 2 microns in size in the ELI alloys. Variations in cooling rate did not seem to affect its size or volume fraction. These particles are similar in appearance to those previously reported to be the iron-stabilized β phase,[3,4] but no investigation has determined both the particle composition and its crystal structure. Microprobe analysis and TEM diffraction were used to identify this phase. Microprobe analysis of particles in the air-cooled normal interstitial alloys showed that the iron content was 6.5 weight percent with a standard deviation of 0.5 percent. When this is compared to the bulk check iron analysis of 0.30 percent given in Table I, it is obvious that this phase is very enriched in iron. The particles in the ELI alloy were too small for quantitative analysis, but the iron x-ray intensity increased when the microprobe electron spot was on a particle.

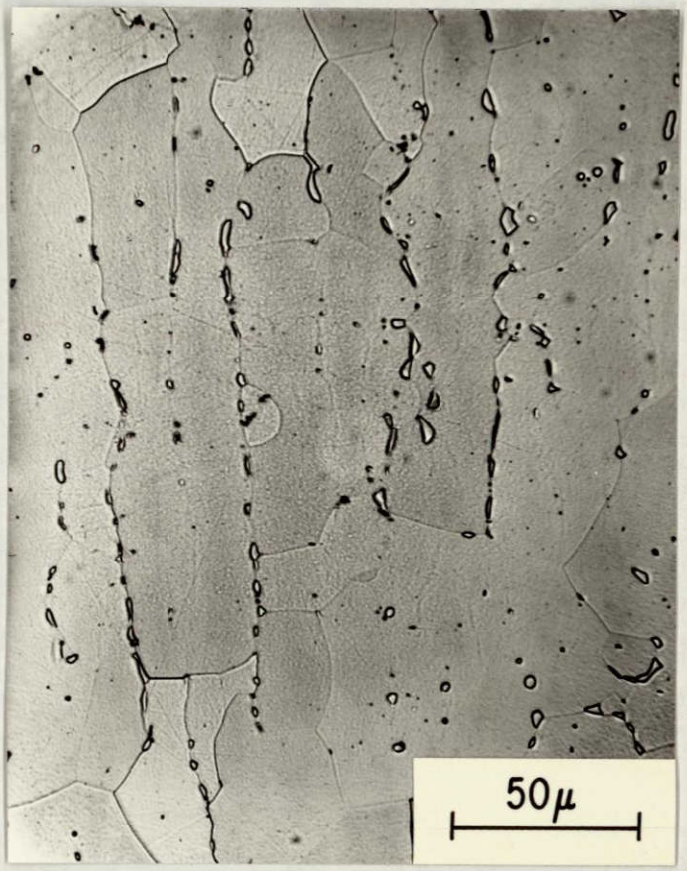

Figure 1. Bright-Field Optical Micrograph of Furnace-Cooled Normal Interstitial Ti-5Al-2.5Sn Plate. The longitudinal direction is vertical and the short transverse direction is horizontal.

TABLE II

Intercept Grain Sizes of Ti-5Al-2.5Sn Alloys

Alloy	Average Intercept Grain Size (μm)	Standard Deviation of Intercept Grain Size (μm)
ELI, Air-Cooled	46.2	4.3
ELI, Furnace-Cooled	58.1	4.0
Normal Interstitial, Air-Cooled	41.6	4.2
Normal Interstitial, Furnace-Cooled	41.4	4.0

This phase was retained in thin foils of the normal interstitial alloys prepared for TEM. Electron diffraction patterns of the furnace-cooled normal interstitial particles could be indexed at the β phase with a lattice parameter equivalent to a titanium - 6.5 percent iron β alloy.[22] Within the air-cooled particles there was a precipitate present. The diffraction patterns of these particles could be indexed as α precipitation with the Burger's crystallographic orientation ($\langle 11\bar{2}0\rangle_\alpha \,||\, \langle 111\rangle_\beta$ and $(0001)_\alpha \,||\, \{111\}_\beta$) to the β particle matrix. This difference in internal structure of the iron-stabilized β phase probably results from variations in cooling rate. In furnace-cooled alloys, the α stabilizing elements in the β phase can diffuse to the perimeter of the particle where the α forms. In other words, the size of the β particle will shrink during furnace cooling. In the air-cooled material, the temperature apparently decreases too rapidly for extensive diffusion to occur, so α precipitates within the β. The only observation of the β phase in ELI alloys was in the furnace-cooled plate where no α precipitation was observed.

Thin foil TEM was also used to determine if the α matrix of the Ti-5Al-2.5Sn alloys was ordered. Since the ordering behavior in the ELI and normal interstitial alloys was identical, only the results from the ELI plates will be given. Figure 2 shows electron diffraction patterns of the α matrix of air-cooled and furnace-cooled ELI alloys. The zone axis for both patterns is identical and is close to $(4\bar{5}15)$. The pattern from the furnace-cooled material has extra spots which can be indexed as the α_2 phase. These superlattice reflections lacked sufficient intensity to obtain a dark field image of the precipitates. The presence of the superlattice reflections and the absence of a dark field image confuses the description of the microstructures. The classical approach would be to

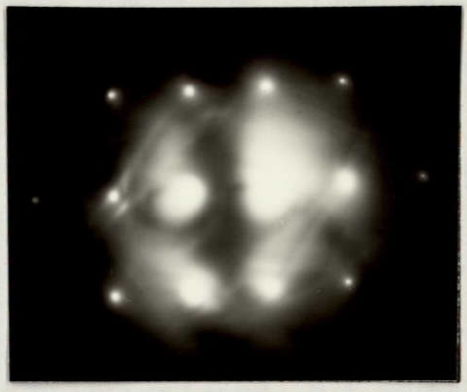

(a) Air-Cooled

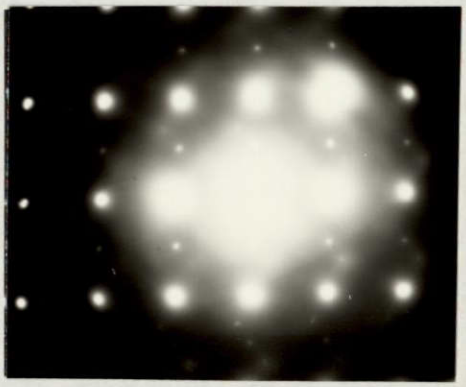

(b) Furnace-Cooled

Figure 2. SAD Patterns of ELI Ti-5Al-2.5Sn Alloys.

cooled ELI alloy when the grain size is slightly larger. The alloy purity affected the dispersion of the iron-stabilized β phase and crystallographic texture. The normal interstitial alloys with their higher iron content had a larger size and volume fraction of the β phase than ELI material. The ELI alloys have a basal texture while the normal interstitial plates have a β processing texture. The changes in cooling rate altered the ordering characteristics of the α matrix and the internal structure of the β phase. The air-cooled β phase had α precipitation within it while the furnace-cooled β phase was free of α precipitation. Both furnace-cooled alloys were ordered while electron diffraction of the air-cooled materials showed no evidence of ordering.

MECHANICAL PROPERTIES

The tensile properties and plane strain fracture toughness (K_{Ic}) of the Ti-5Al-2.5Sn alloys were determined at room temperature (295°K or 72°F), liquid nitrogen temperature (77°K or -320°F), and liquid hydrogen temperature (20°K or -423°F). The techniques and test results have been described elsewhere[25] and will be summarized here. The fracture toughness specimens had a normal thickness of 25 mm (1 inch). Compact tension specimens were used at 77°K and 295°K while three-point bend specimens were used at 20°K. Figure 3 shows the variation in longitudinal yield strength, longitudinal ultimate tensile strength, and LT orientation fracture toughness for the Ti-5Al-2.5Sn alloys with test temperature. In LT orientation fracture toughness specimens, the crack plane is perpendicular to the longitudinal direction and the crack propagates in the transverse direction so the plane of fracture had the same orientation in all specimen geometries. The error bars in

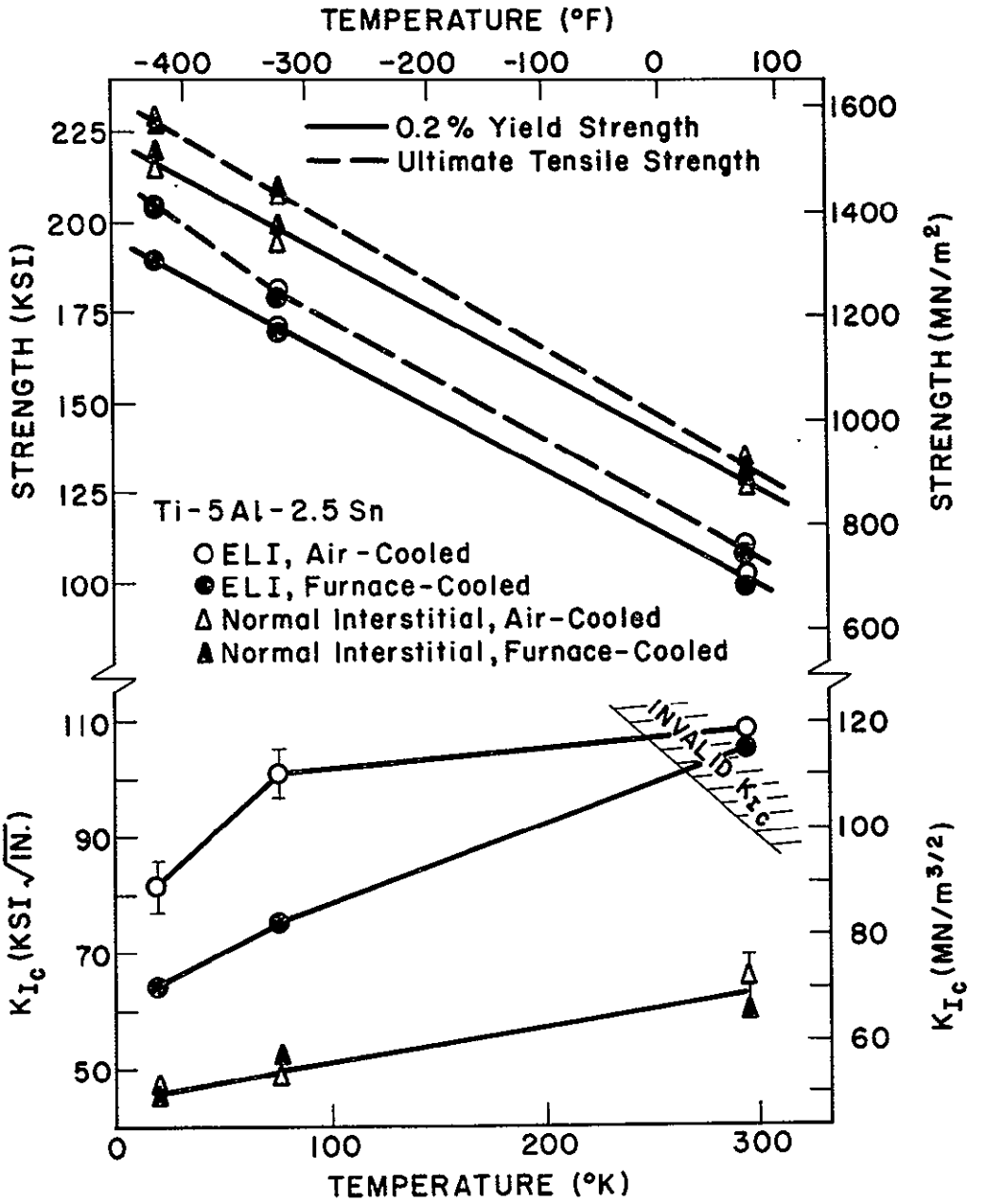

Figure 3. Variation of Longitudinal Tensile Properties and LT Fracture Toughness of Ti-5Al-2.5Sn with Test Temperature. The error bars indicate the range of plus and minus one standard deviation.

Figure 3 indicate the range of plus and minus one standard deviation (68 percent confidence limits) calculated from multiple tests. The room temperature fracture toughness data of the ELI alloys are invalid due to the thickness criteria of the current ASTM test method[26] and represent the results of single tests.

As one would expect, the strength level of the normal interstitial alloys are about 175 MN/m^2 (25 ksi) higher than the ELI alloys. In most cases, the ultimate tensile strength is 70 MN/m^2 (10 ksi) higher than the yield strength. For both grades, the yield strength at 20°K is approximately twice that of room temperature. Both the yield strength and ultimate tensile strength decrease in a linear fashion with increasing test temperature. Variations in cooling rate had no significant influence on strength levels.

The ELI alloys are much tougher than those of the normal interstitial alloys. Cooling rate from the annealing temperature has no significant effect on the toughness of the normal interstitial plates, but the air-cooled ELI material has a K_{Ic} approximately 30 percent greater than the furnace-cooled ELI alloy at 20°K and 77°K. The test record of the furnace-cooled ELI specimen at room temperature had a lower load and crack mouth displacement than the air-cooled ELI specimen at the onset of fast fracture. This suggests that at room temperature, the air-cooled ELI alloy is tougher than the furnace-cooled ELI alloy even though the toughness assessed by the ASTM secant offset method[26] are similar.

The tensile fracture strains decreased with increased interstitial levels and lower test temperature. The fracture strains were not significantly affected by cooling rate. Comparison of tensile ductility data with K_{Ic} values points out the danger of trying to qualitatively assess the toughness of titanium alloys with tensile ductility data.

Tensile flow curves were determined for the Ti-5Al-2.5Sn alloys at strains above and below the strain required for necking. Changes in cooling rate had no influence on flow curves. The difference in flow curves between the ELI and normal interstitial alloys resulted largely from increasing yield strength with decreasing alloy purity. The work-hardening rate decreased with increasing strain but was not affected by composition and cooling rate. Decreases in test temperature increased the work-hardening rate. Similar observations have been made by Conrad, et al.[27] in unalloyed titanium.

FRACTOGRAPHY

The fracture surfaces of tensile and fracture toughness specimens tested at all three temperatures were observed using two-stage TEM replicas as well as the scanning electron microscope (SEM). The room temperature fracture surfaces were covered almost totally by equiaxed dimples. At 20°K and 77°K, a large portion of the fracture surfaces were covered by elongated dimples. Figure 4 shows a TEM replica fractograph of a furnace-cooled ELI Ti-5Al-2.5Sn fracture toughness specimen tested at 77°K with equiaxed dimples in Region A and elongated dimples in Region B. The equiaxed dimples are up to 10 microns in diameter. The elongated dimples are up to 10 microns in width dimension. The use of stereo pairs show that the elongated dimples tend to be more shallow than the equiaxed dimples. The primary distinguishing feature in the elongated dimples is the shallow depression along the dimple length. It is interesting to note that the equiaxed dimple labeled A has a fine depression similar to those observed in the elongated dimples.

Figure 5 shows a TEM replica fractograph of an air-cooled normal interstitial fracture toughness specimen tested at 77°K. This fractograph

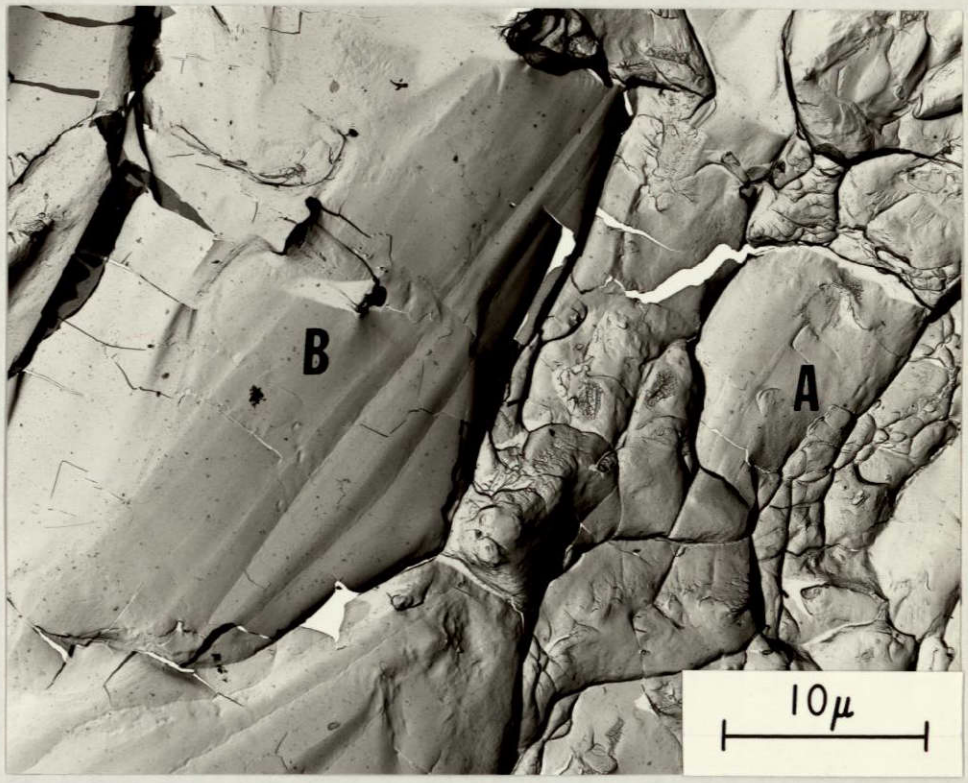

Figure 4. TEM Replica Fractograph of a Furnace-Cooled ELI Ti-5Al-2.5Sn Fracture Toughness Specimen Tested at 77°K. Regions of equiaxed and elongated dimples are labeled "A" and "B", respectively.

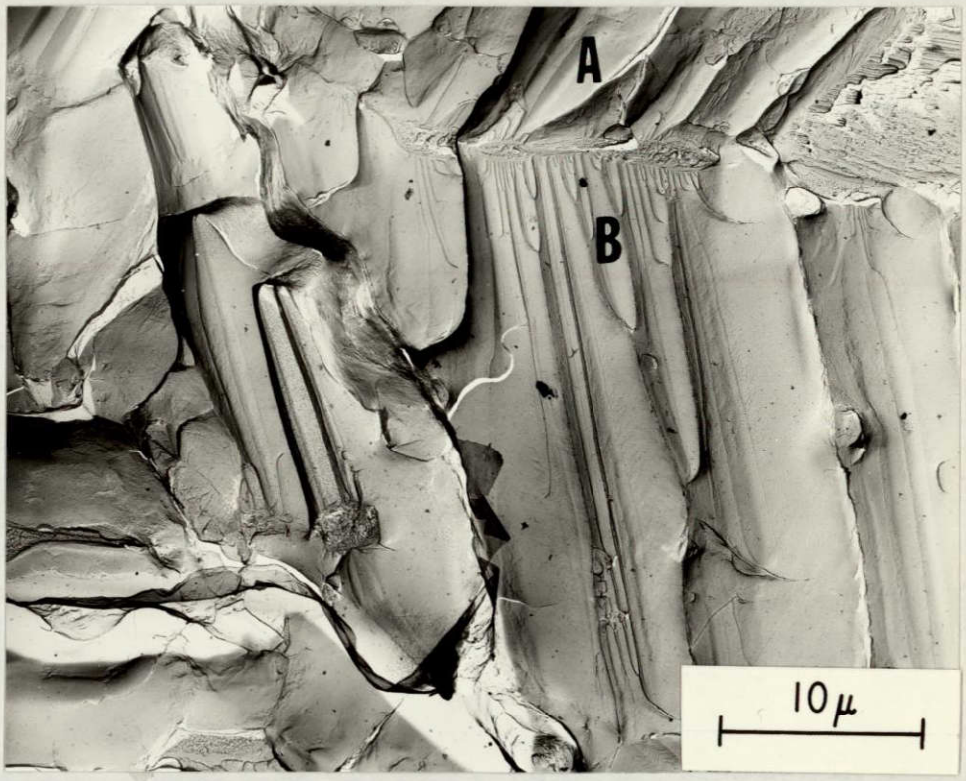

Figure 5. TEM Replica Fractograph of an Air-Cooled Normal Interstitial Ti-5Al-2.5Sn Fracture Toughness Specimen Tested at 77°K. Regions "A" and "B" have different orientations of elongated dimples.

shows a region covered almost totally with elongated dimples. These dimples and their associated depressions seem to form in localized regions with their lengths aligned in one direction. Regions A and B in Figure 5 show two such regions with different orientations which are separated by a fairly distinct boundary. This observation suggests that these features are related in some fashion to the crystallography of the α matrix so that discontinuities in crystal structure such as grain boundaries will terminate the dimples.

The TEM replicas were viewed using stereo pairs and the equiaxed and elongated dimples always appeared to be dimples. SEM fractography of mating fracture surfaces from an air-cooled ELI fracture toughness specimen was used to show that the elongated dimples match peak to peak. Thus, it seems just prior to fracture the elongated were tubular in shape. Similar fractographic features have been observed on stress corrosion failures of titanium[2, 28, 29] and zirconium alloys[30] between cleavage planes and are often called "flutes". Aitchison and Cox[30] performed mating surface fractography and showed that their "flutes" also resulted from tubular voids. It is generally accepted, but has never been proven, that these features on stress corrosion failures result from a non-environmentally assisted strictly mechanical failure mechanism. This contention was supported by the observation of these features on the fracture surfaces of Ti-5Al-2.5Sn and titanium-oxygen alloys[17] broken at cryogenic temperatures.

The fracture surfaces of Ti-5Al-2.5Sn specimens tested at 20°K and 77°K appeared to be similar within a given alloy. Over this temperature range there was no evidence of discontinuities in mechanical properties. This suggests that the influence of microstructure on the

fracture mechanism is similar at 20°K and 77°K. Any recommended change in microstructure to improve K_{Ic} at 77°K would be expected to have a similar effect on the 20°K toughness. Thus, the investigation was restricted to study the fracture mechanism at 77°K.

The fracture surfaces of tensile and fracture toughness specimens tested at 77°K were studied in the SEM. Figure 6 shows an SEM fractograph from a region of an air-cooled ELI fracture toughness specimen just ahead of the fatigue precrack. The macroscopic direction of crack propagation is from left to right. The fracture surface is a mixture of equiaxed and elongated dimples. Elongated dimples in Figure 6 are oriented anywhere from parallel to perpendicular to the crack propagation direction. Thus, it does not appear that the elongated dimples are related to stress state.

The SEM fractograph were analyzed in a quantitative fashion so as to observe if there are any systematic variations from alloy to alloy or between tensile specimens and fracture toughness specimens. The areal fraction, number per unit area, length, width, and aspect ratio of the elongated dimples were measured. Table III gives the average and standard deviations of the quantitative fractography data on the elongated dimples. Although the standard deviations of the areal fraction data are quite large, it appears that roughly half the fracture surfaces of both types of specimens for all four alloys are covered by elongated dimples.

The major difference in the fracture surfaces are the density and size of the elongated dimples. Increases in K_{Ic} seem to be associated with decreases in the number of elongated dimples. As one might expect for a relatively constant areal fraction, increases in the number of elongated dimples result in reduction of their size. The standard deviations on dimple size are quite large so the cumulative dimple length and

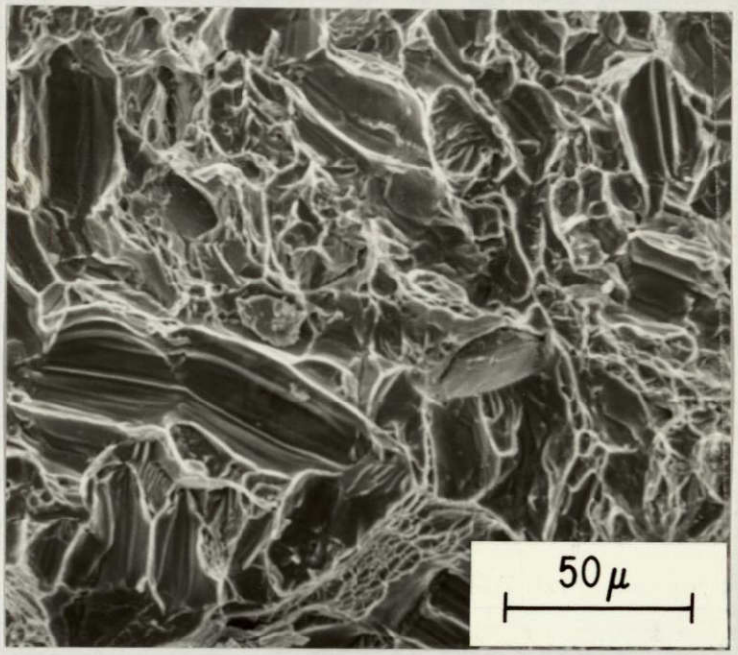

Figure 6. SEM Fractograph of an Air-Cooled ELI Ti-5Al-2.5Sn Fracture Toughness Specimen Tested at 77°K. The crack propagation direction is from left to right.

TABLE III

Quantitative Fractography of the Elongated Dimples Observed on Ti-5Al-2.5Sn Specimens Tested at 77°K

Alloy	Specimen Type	Areal Fraction	Number Per Unit Area (10^3 mm^{-2})	Dimple Length (μm)	Dimple Width (μm)
ELI, Air-Cooled	K_{Ic}	0.564 ± 0.095	1.85 ± 0.34	25.6 ± 12.7	12.3 ± 5.6
	Tensile	0.350 ± 0.078	1.73 ± 0.37	22.0 ± 10.7	11.5 ± 6.4
ELI, Furnace-Cooled	K_{Ic}	0.450 ± 0.094	2.13 ± 0.39	20.4 ± 12.2	9.3 ± 4.4
	Tensile	0.389 ± 0.077	2.08 ± 0.32	19.2 ± 10.3	8.4 ± 4.8
Normal Interstitial, Air-Cooled	K_{Ic}	0.423 ± 0.039	3.11 ± 0.50	16.8 ± 9.5	6.4 ± 2.9
	Tensile	0.427 ± 0.047	3.57 ± 0.55	17.8 ± 10.0	6.9 ± 3.2
Normal Interstitial, Furnace-Cooled	K_{Ic}	0.472 ± 0.084	3.24 ± 0.85	17.1 ± 9.7	6.5 ± 3.1
	Tensile	0.521 ± 0.103	3.90 ± 0.60	15.5 ± 8.5	6.2 ± 3.2

width distributions were determined. The distributions of the fracture toughness specimens are given in Figure 7. These data are normalized with respect to the total number of dimples so that all the curves terminate at a frequency of unity. As in the data given in Table III, the dimple size distributions show that the tougher alloys have larger dimples. The two normal interstitial plates which have very similar K_{Ic} values have almost identical size distributions. It is interesting to note that most of the dimples have dimensions smaller than the 45 to 60 micron α intercept grain size of the Ti-5Al-2.5Sn alloys. This adds further support to the suggestion that the elongated dimples may be related to crystallography of the α matrix.

The size distributions of tensile and fracture toughness specimens were different by no more than 2 microns. This information along with the data shown in Table III strongly suggests that the influence of microstructure on the fracture mechanisms is similar in both types of specimens. Due to this similarity, metallographic sectioning experiments were conducted only on tensile specimens. This will avoid the large and relatively unknown stress and strain gradients at a crack tip and will provide a larger region for metallographic observation.

SECTIONING EXPERIMENTS

It is impossible from fractography alone to determine the source of the elongated dimples and the mechanism of how they form, so a series of tensile specimens from each plate were deformed at 77°K to various strains up to including that required for fracture. These specimens were sectioned to their midplanes on a plane parallel to the plate surface and prepared for metallographic observation. After necking occurred, only

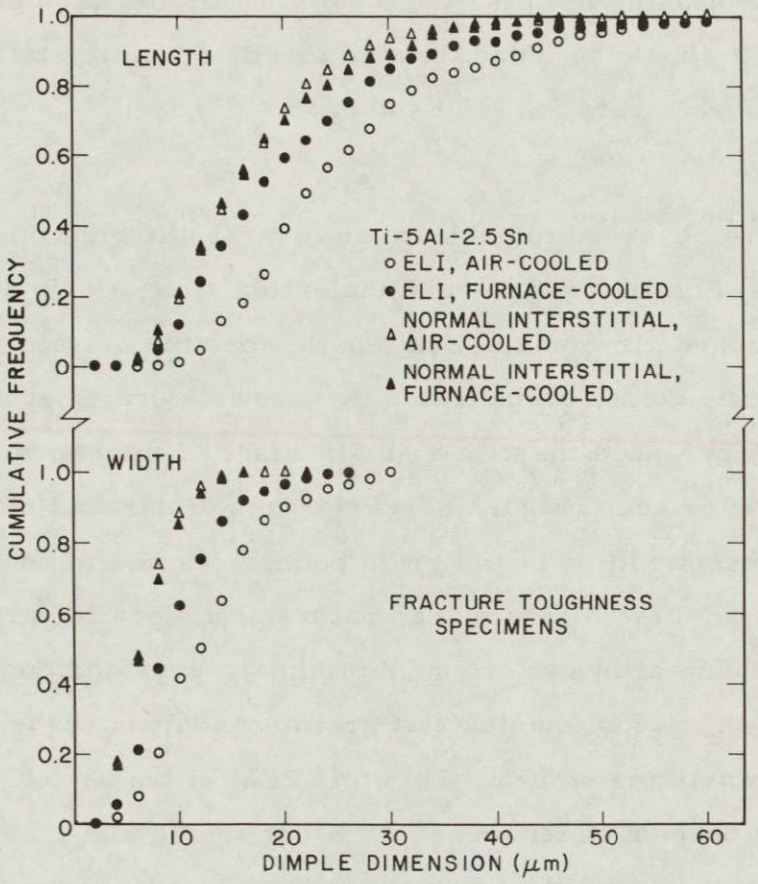

Figure 7. Length and Width Distributions of the Elongated Dimples of the Ti-5Al-2.5Sn Fracture Toughness Specimens Tested at 77°K.

the necked region was studied. The optical microscope and SEM were used to study the void nucleation, void growth, and void coalescence processes in Ti-5Al-2.5Sn at 77°K. During the presentation of the metallographic sectioning results, the plastic strain for each micrograph is given. It should be noted that the tensile fracture strain for these alloys at 77°K is between 0.30 and 0.35.

Void Nucleation

Voids were observed to nucleate at several different microstructural sites. Figure 8 shows void nucleation along a primary twin boundary in sectioned air-cooled, ELI tensile specimen strained to 0.348 at 77°K. The voids, as indicated by arrows, formed at regions of the twin boundary where there is a small offset or displacement in the twin-matrix interface. Figure 8 has two sets of parallel etched bands which intersect with twin and grain boundaries and in some cases, apparently cause an offset. The planar nature of dislocation arrays in titanium-aluminum alloys at cryogenic temperatures and the observation that most of the bands terminate at grain boundaries suggests that slip bands are sometimes etched. Thin foil TEM of the Ti-5Al-2.5Sn alloys strained 3 percent in tension at 77°K confirmed that the dislocations form in planar slip bands that are similar in appearance to those reported in other titanium-aluminum alloys.[10]

The metallographic surface shown in Figure 8 was repolished and etched two times in order to determine if the offsets and voids exist along the entire length of the deformation twin. The surfaces observed by serial sectioning were 21 and 26 microns below that shown in Figure 8. The two voids, offsets in the twin boundaries, and two sets of etched bands shown in Figure 8 were also observed on the serial sectioned surfaces. This shows that these voids have tubular shapes and

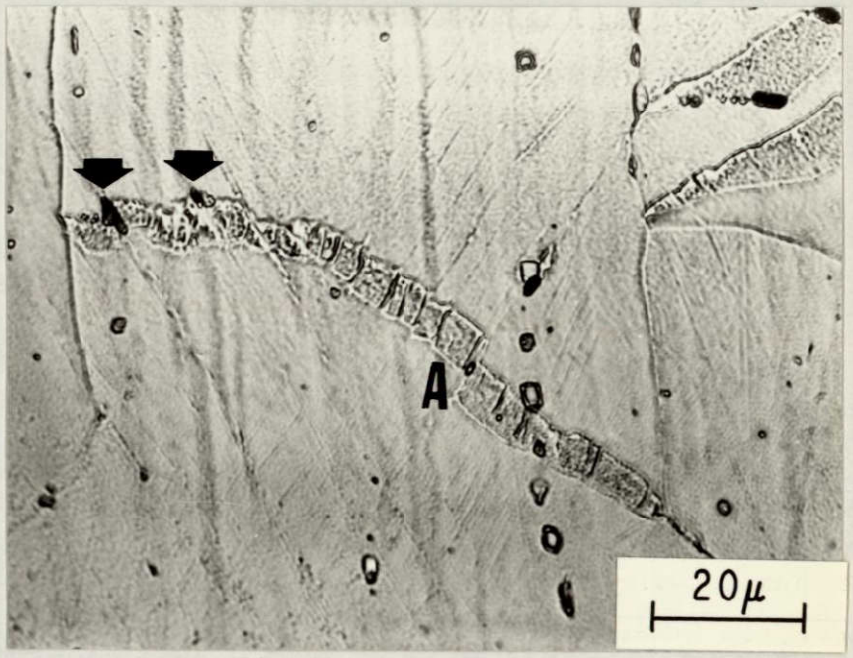

Figure 8. Offsets and Void Nucleation along Primary Twin Boundaries in an Optical Micrograph of a Sectioned Air-Cooled ELI Ti-5Al-2.5Sn Tensile Specimen Strained to 0.348 at 77°K. The arrows point to voids along the primary twin boundary at offsets. The letter "A" indicates an offset without void nucleation. The tensile axis is vertical.

that both offsets and voids extend over large lengths. The observation events showed that the voids always terminated as they crossed a grain boundary. It was also observed that some voids terminated within a grain even though the offset region continued to the grain boundaries. Thus, it was confirmed that offsets in twin boundaries are void nucleation sites and that offsets form before void nucleation occurs. This is demonstrated in Figure 8 where no void is observed at the offset labeled A. It should be noted that the magnitude of offset A normal to the twin may be much smaller than observed in Figure 8 because the twin boundary may make a small angle with the metallographic surface.

Thin foil TEM of the Ti-5Al-2.5Sn alloys deformed 3 percent in tension at 77°K confirmed that slip bands can cause offsets in twin boundaries. The TEM micrograph in Figure 9 shows several places where slip bands have caused small displacement of the primary twin boundary. The largest offset is indicated with an arrow. These offsets are quite small but do show that a blocked slip band can cause offsets in the twin boundary. It is important to note that the sectioned specimen shown in Figure 8 had a macroscopic strain an order of magnitude larger than of the thin foil in Figure 9.

Void nucleation was also observed at offsets at α grain boundaries. Figure 10 shows such offsets in a furnace-cooled ELI tensile specimen strained to 0.326. Several voids can be observed at the grain boundary offsets in Figure 10. These offsets form at the intersection between etched bands and a grain boundary, suggesting that they form from the intense shear of a planar slip band.

Another void nucleation site is at the intersection of multiple twins. Figure 11 is an SEM micrograph with an example of this type

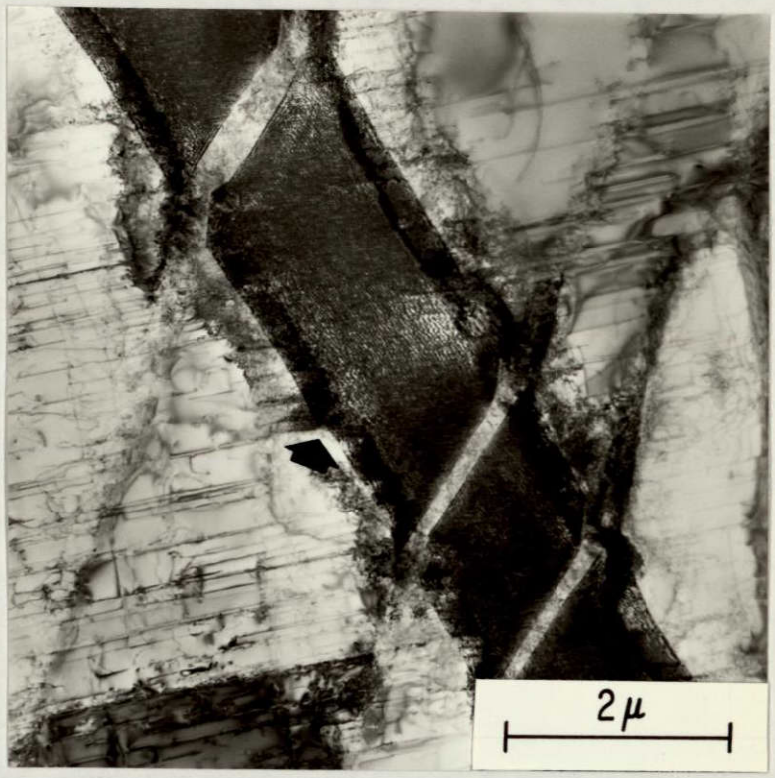

Figure 9. Thin Foil TEM Micrograph Showing an Offset at the Intersection of a Slip Band with a Primary Twin Boundary.

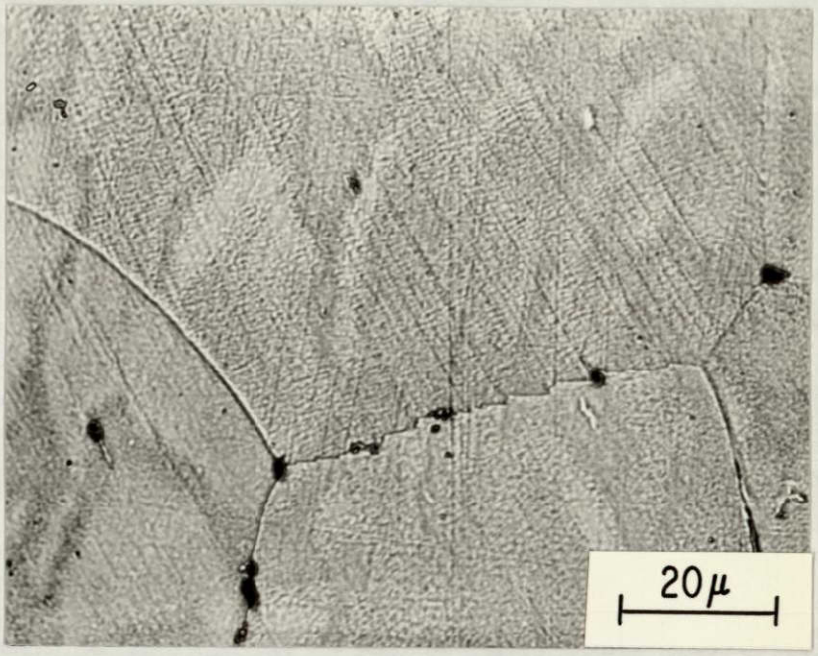

Figure 10. Optical Micrograph Showing Offsets and Void Nucleation at a Grain Boundary in a Sectioned Furnace-Cooled ELI Ti-5Al-2.5Sn Tensile Specimen Strained to 0.326 at 77°K. The tensile axis is vertical.

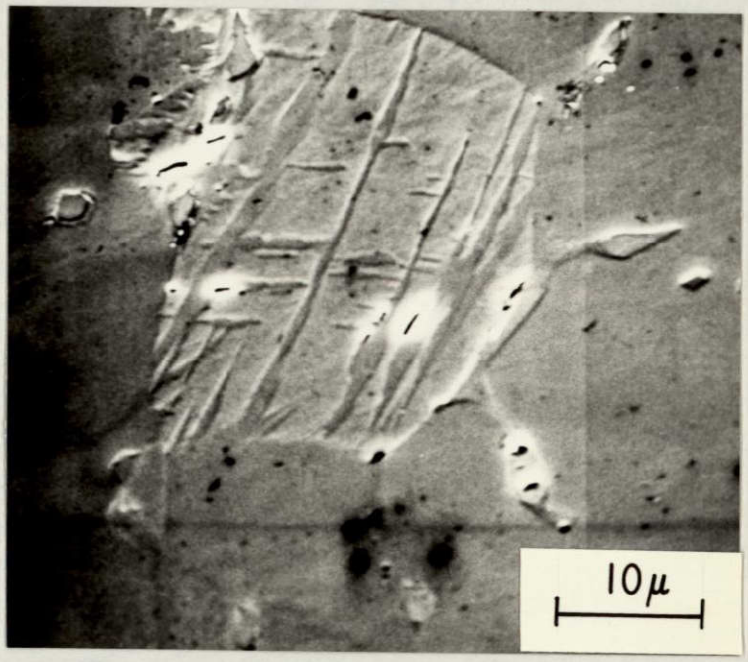

Figure 11. SEM Micrograph Showing Void Nucleation at Multiple Twins in a Sectioned Air-Cooled Normal Interstitial Ti-5Al-2.5Sn Tensile Specimen Strained to 0.243 at 77°K.

of void nucleation in an air-cooled normal interstitial tensile specimen with 0.243 plastic strain. The voids in this micrograph are white because alumina polishing compound, which does not conduct electrons, is in the cavities. No offset could be observed at multiple twin intersections prior to void nucleation using the optical microscope or the SEM on sectioned specimens; however, such offsets were observed using thin foil TEM. Figure 12 shows a TEM micrograph of multiple twin intersection in an air-cooled normal interstitial Ti-5Al-2.5Sn tensile specimen strained 3 percent at 77°K. This micrograph shows the large density of accommodation dislocations along the twin boundaries. They are especially numerous in the vicinity of the twin intersection. Based on these offsets and large strain concentrations, it is not surprising that multiple twin intersections are sites for void nucleation. Such offsets have been previously observed when twins with different crystallographic shear directions intersect.[31]

Void nucleation also occurred at the iron-stabilized β phase. Figure 13 shows an example of this type of void nucleation in a furnace-cooled normal interstitial tensile specimen with a plastic strain of 0.128. Voids generally formed by the decohesion of the interface between the β particle and the α matrix. These voids formed at the regions of the interface normal to the tensile axis of the specimens. This behavior is similar to that in some other materials[32] which fail by classical dimpled rupture.

Void Growth

The void growth process in Ti-5Al-2.5Sn alloys at cryogenic temperatures is quite different than that observed in classical dimpled rupture. In the case of the cavities which nucleate along deformation twins or grain boundaries, the voids grow along the boundaries with relatively

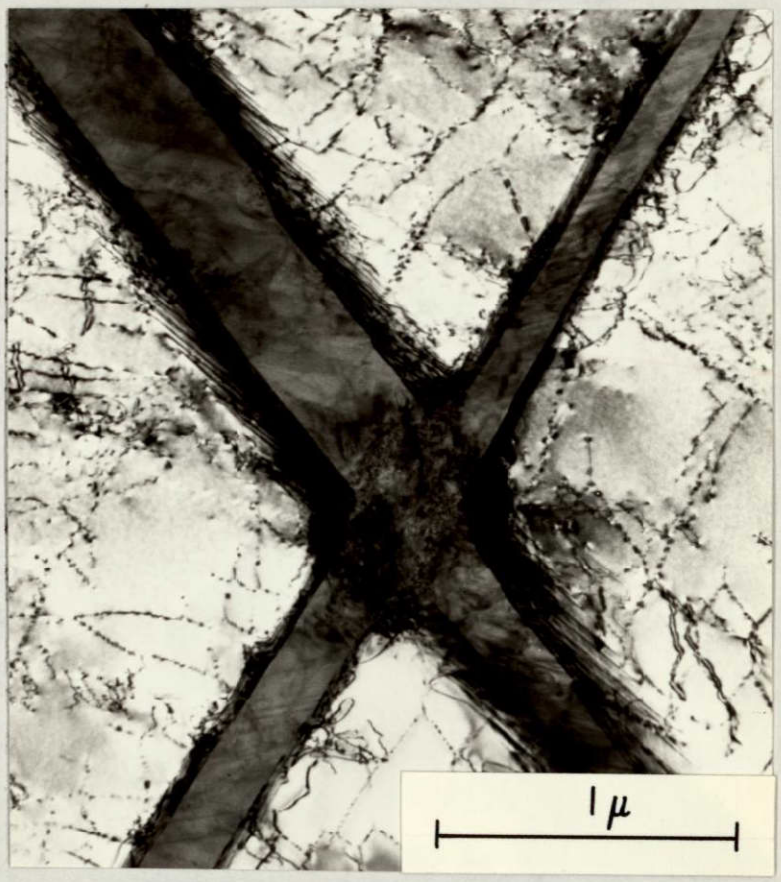

Figure 12. Thin Foil TEM Micrograph Showing a Multiple Twin Intersection in Air-Cooled Normal Interstitial Ti-5Al-2.5Sn Strained 3 Percent in Tension at 77°K.

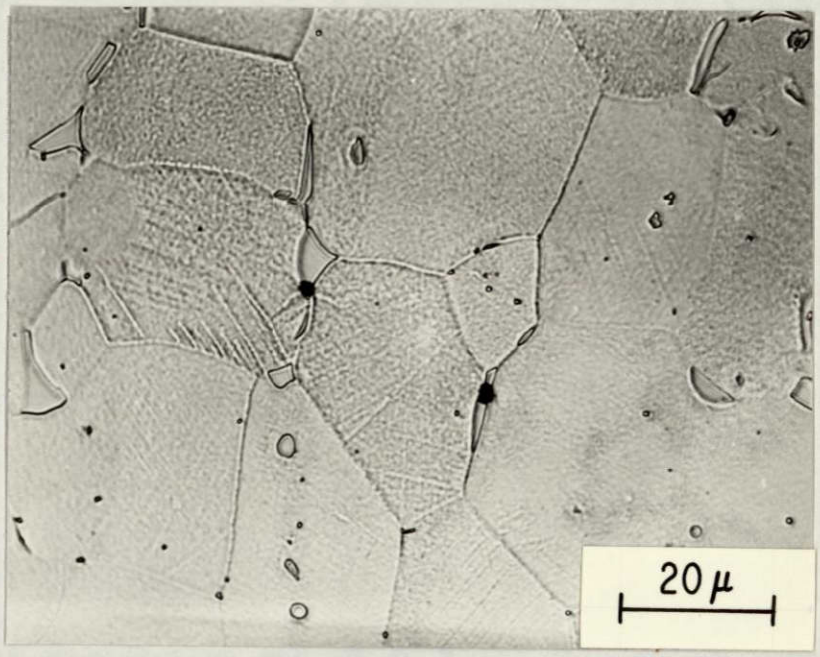

Figure 13. Optical Micrograph Showing Void Nucleation at β Particles in a Sectioned Furnace-Cooled Normal Interstitial Ti-5Al-2.5Sn Tensile Specimen Strained to 0.128 at 77°K. The tensile axis is vertical.

little growth into the matrix. Figure 14 shows this type of void growth along a primary twin in a furnace-cooled normal interstitial tensile specimen with a plastic strain of 0.326. Voids which nucleate at iron stabilized β particles not on boundaries grow into roughly spherical cavities which are much smaller than the twin or grain boundary voids. Several voids at boundaries apparently nucleated at the β phase and subsequently grew along the boundary. The observations of void nucleating particles in the bottoms of some of the elongated dimples on the fracture surfaces suggest that the β phase may nucleate such voids.

Void Coalescence

The mechanism of void coalescence in the Ti-5Al-2.5Sn alloys was by the impingement of voids growing along boundaries and at β phase particles. Figure 15 shows an example of this phenomena in a furnace-cooled normal interstitial tensile specimen with a plastic strain of 0.326 where voids nucleated at multiple twins and β phase are in the process of coalescing by impingement. No evidence of void sheet formation[32,33,34] or any other intervening fracture mechanism was observed.

Quantitative Sectioning Studies

The three stages of the fracture process in Ti-5Al-2.5Sn alloys at 77°K have been described in a qualitative fashion; however, to fully understand the influence of composition and microstructure on fracture toughness, the fracture mechanism must be described in a more quantitative manner. The central region in tensile specimens 2 mm (0.008 in.) wide and 3 mm (0.12 in.) in the axial direction was studied using quantitative metallography. This size was picked to avoid the shear lip

Figure 14. Optical Micrograph Showing Void Growth Along Primary Twin Boundaries in a Sectioned Furnace-Cooled Normal Interstitial Ti-5Al-2.5Sn Tensile Specimen Strained to 0.326 at 77°K. The tensile axis is vertical.

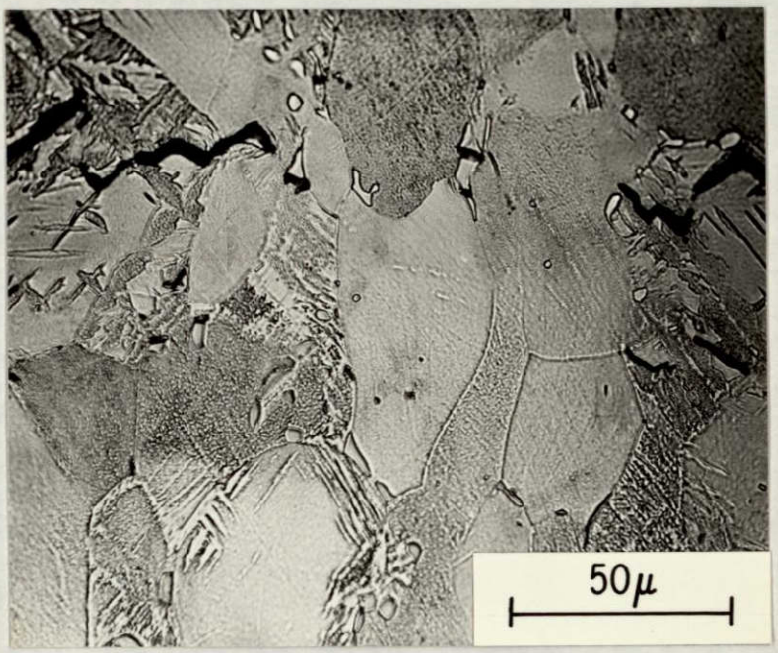

Figure 15. Optical Micrograph Showing Void Coalescence in a Sectioned Furnace-Cooled, Normal Interstitial Ti-5Al-2.5Sn Tensile Specimen Strained to 0.326 at 77°K. The tensile axis is vertical.

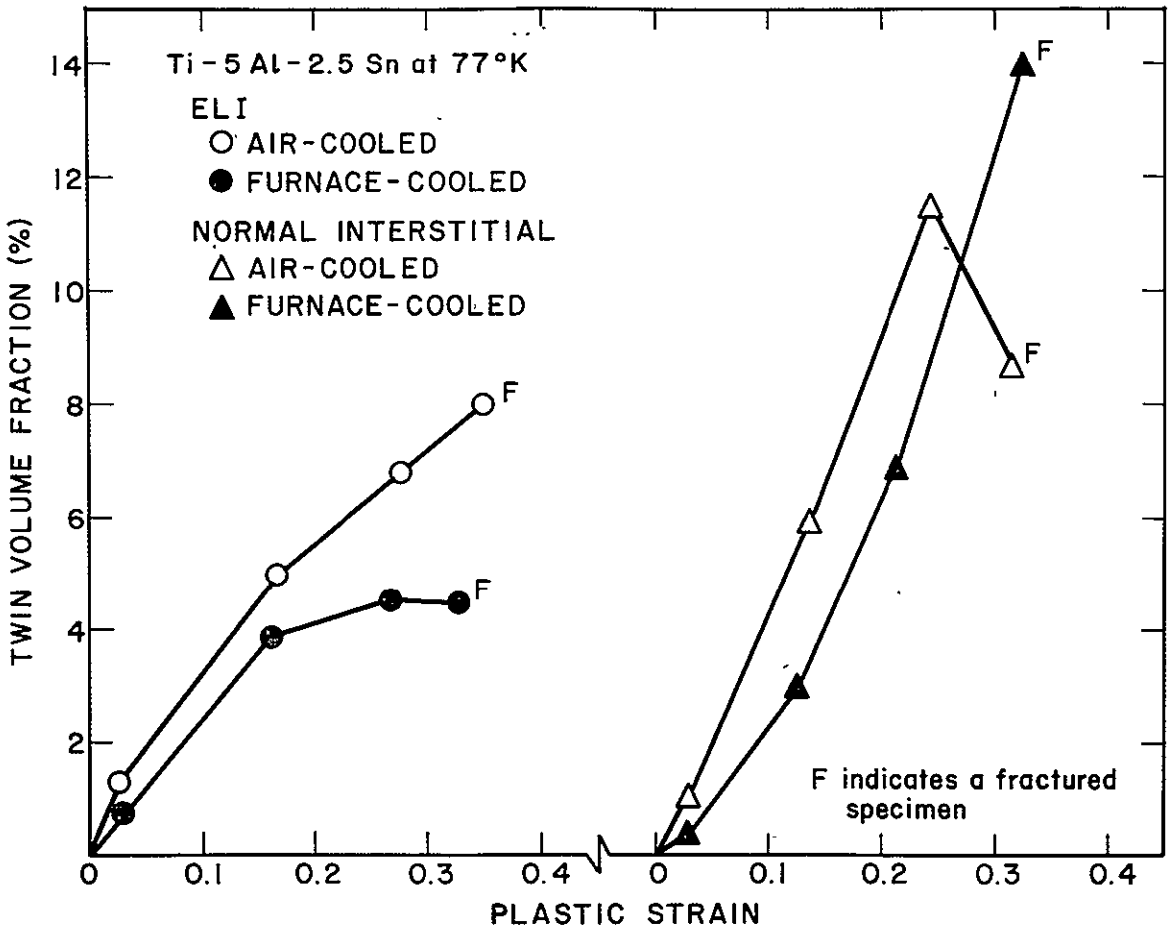

Figure 16. Variation of the Twin Volume Fraction of the Ti-5Al-2.5Sn Alloys with Plastic Strain at 77°K.

interstitial plates with a β processed texture have a high resolved shear stress on $(10\bar{1}2)$, $(11\bar{2}1)$, $(11\bar{2}2)$, $(11\bar{2}3)$, and $(11\bar{2}4)$ twin systems. Reed-Hill[35] showed that in polycrystalline zirconium that the variation in the number of twins is very similar in shape to the variation in resolved shear stress. Based on this, one would expect only $(11\bar{2}2)$ twinning in the ELI alloys; but all five twin systems would operate in the normal interstitial alloys. The quantitative sectioning data showed that about 75 percent of the twins in the ELI specimens were primary twins while in the normal interstitial materials, approximately 75 percent of the twins were multiple twins. This supports the resolved shear stress calculations. It is not surprising then that the normal interstitial alloys with several more highly stressed twin systems have higher twin volume fractions.

Figure 16 shows that the furnace-cooled plate of both compositions have a lower twin volume fraction than the air-cooled materials at equivalent strains. The twin volume fraction in the more slowly cooled plates is probably due to the order in those materials. This effect has been observed in ordered stoichiometric compounds such as Mg_3Cd[36] but has not been investigated in nonstoichiometric ordered alloys. The cause of this behavior is not known but may be due to changes in atomic arrangements which accompany twinning.[37]

The ordering in the normal interstitial plates has less influence on the twin frequency than in the ELI materials. A similar observation was made of the dislocation arrangements when material of each alloy strained 3 percent in tension was studied using thin foil TEM. The dislocations in all the alloys were very planar. In the air-cooled ELI alloy, the dislocations had a fairly uniform distribution; while in the furnace-cooled ELI material, the dislocations were spaced in a less uniform

fashion and started to form intense slip bands. In the normal interstitial alloys, the dislocations were in very intense slip bands spaced on the order of one micron apart. Cooling rate did not greatly affect the slip band spacing in the less pure plates. The observations of increased slip band spacing with ordering and higher interstitial content have been reported previously in titanium-aluminum alloys.[10,11]

Figure 17 shows the total number of voids per unit area as a function of plastic strain for the Ti-5Al-2.5Sn alloys. Void nucleation in the toughest alloy, the air-cooled ELI material, does not occur until the plastic strain exceeds 0.15. At this strain, all other alloys have a significant number of voids. Both normal interstitial alloys and the furnace-cooled ELI material have roughly similar void nucleation rates.

In both ELI alloys, over 90 percent of the voids form along primary twin boundaries or grain boundaries. The major difference between these materials is that in the air-cooled ELI specimens, most of the voids form at primary twin boundaries while grain boundaries were the most frequent void nucleation sites in the furnace-cooled ELI alloys. In order to determine if fewer voids form at primary twins in the furnace-cooled ELI alloys due to their lower twin volume fraction, the number of primary twin voids should be plotted as a function of the primary twin volume fraction. Such a plot is shown in Figure 18. At the same volume fraction, the number of voids in the furnace-cooled plate exceeds that of the air-cooled alloy. A similar conclusion can be reached when considering the void nucleation rate at grain boundaries in the ELI alloys. Based on the intercept grain sizes in Table II, the air-cooled ELI alloys have a grain boundary area per unit volume 26 percent greater than the furnace-cooled ELI plate. Even with a smaller amount of potential void

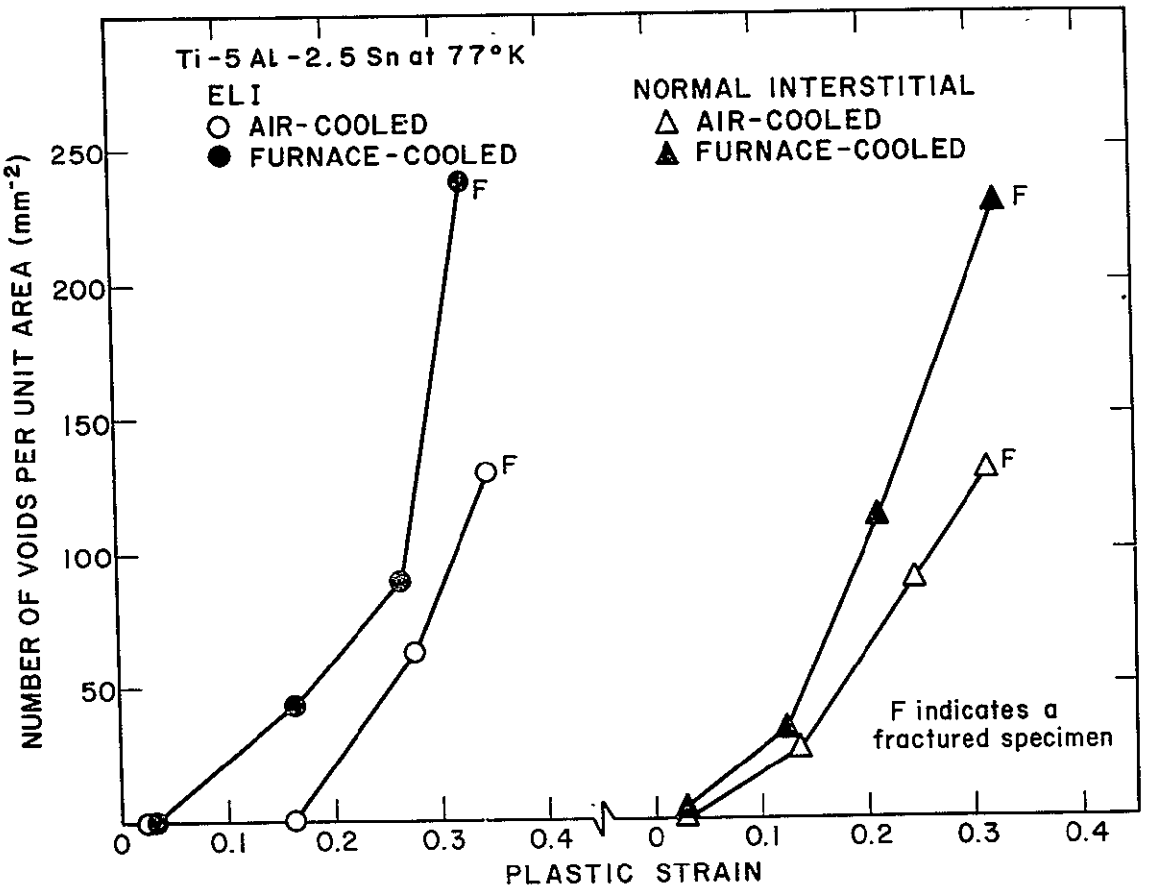

Figure 17. Variation of the Number of Voids per Unit Area for the Ti-5Al-2.5Sn Alloys with Plastic Strain at 77°K.

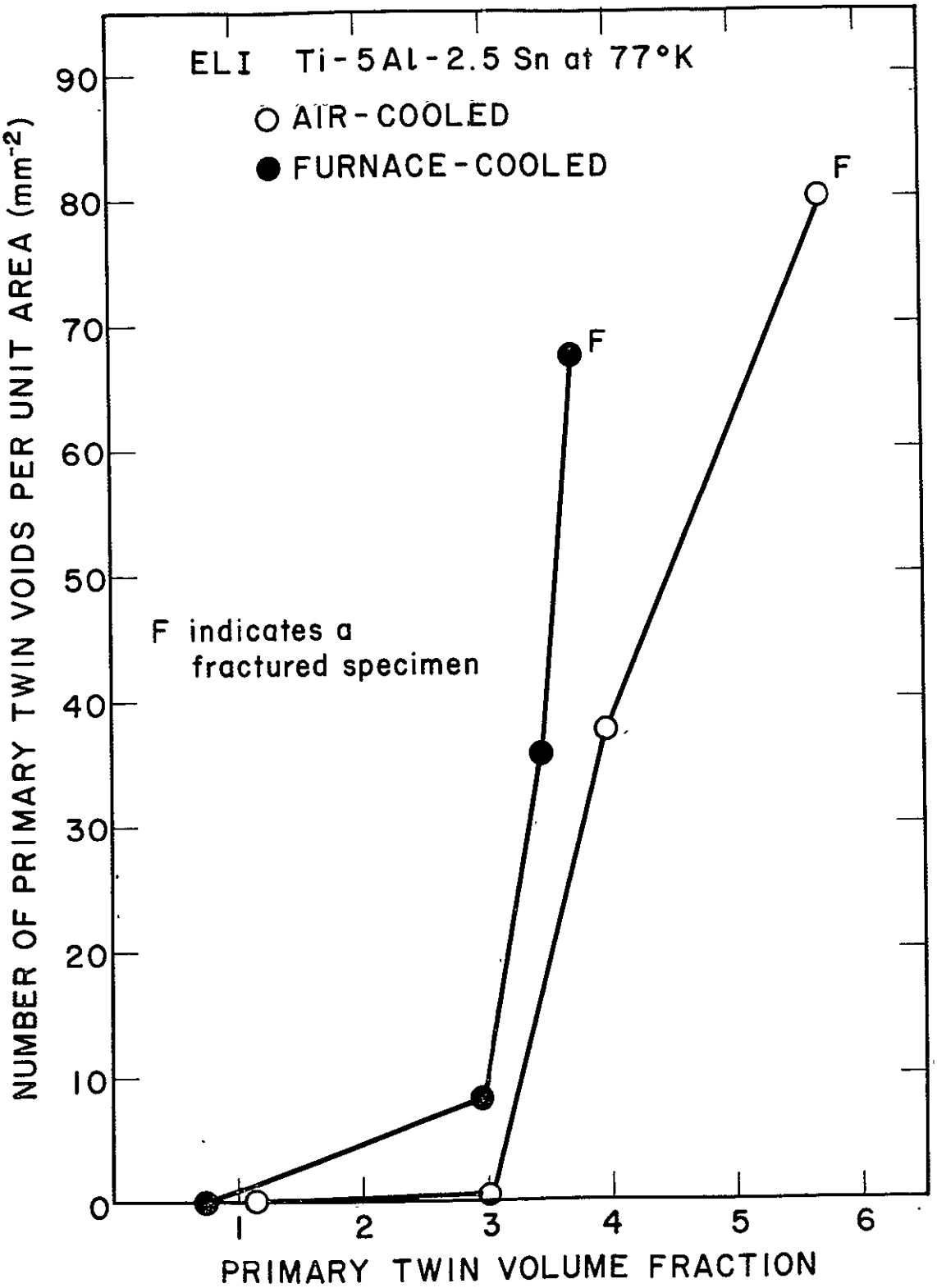

Figure 18. The Number of Primary Twin Voids per Unit Area as a Function of the Primary Twin Volume Fraction for the ELI Ti-5Al-2.5Sn Alloys Strained at 77°K.

nucleation sites, the furnace-cooled ELI material has a greater number of grain boundary voids than the air-cooled alloy. The normalized rates of primary twin and grain boundary void nucleation in the air-cooled ELI alloy is less than in the furnace-cooled ELI alloys.

In the normal interstitial alloys, most of the voids form at the iron-stabilized β phase particles and multiple twins. These two sites are the ones observed least frequently in the ELI alloys. The reason why voids nucleate at the β particles in the normal interstitial alloys but to no appreciable extent in the ELI plates is probably related to their larger size in the high iron, normal interstitial materials. Similar void initiation - size effects have been observed in steels,[32] aluminum alloys,[38] and α+β titanium alloys.[39] The higher rate of multiple twin void nucleation in the lower purity materials is due to the higher volume fraction of multiple twins in the normal interstitial alloys.

The quantitative sectioning studies showed that at strains up to 0.10, there are many more voids at β particles than at twin or grain boundaries. This, along with SEM fractography of the normal interstitial alloys showing void nucleation sites similar in size to the β phase in the bottom of many of the elongated dimples, suggests that void nucleation at the β phase may aid in the void nucleation at multiple twins.

Quantitative measurements of void nucleation and growth are difficult to obtain in this study due to the cigar-shape of the voids. Interpretation is further clouded because a single void observed on a sectioned specimen may actually consist of a series of smaller voids which have already coalesced. An example of this behavior was shown in Figure 15. One meaningful measure would be comparison of the average of the largest void length on each field of view, determined on sectioned

specimens with the quantitative fractography of elongated dimples. The average void length is defined as the mean of the longest void in all fields of view studied. Figure 19 shows the variation of the average void length of the Ti-5Al-2.5Sn alloys with plastic strain at 77°K. The largest differences in void length are those between the ELI and normal interstitial alloys with the less tough normal interstitial alloys having larger void sizes. On the sectioned specimens, void length generally increased with decreasing toughness while quantitative fractography showed that the dimple size decreased with decreasing toughness. It should be remembered that voids observed on a sectioned specimen may result from several individual dimples which have already coalesced. The different trends between the void lengths measured on sectioned specimens and elongated dimples on the fracture surfaces show that void coalescence occurs at lower strains in the less tough alloys. In the ELI alloys, the void length does not vary significantly with cooling rate while the dimples in the furnace-cooled ELI alloys are smaller than those in the tougher air-cooled ELI material. This shows that voids in the furnace-cooled ELI alloy coalesce at lower strains than the air-cooled ELI alloys.

DISCUSSION

This investigation has shown that the fracture mechanism of Ti-5Al-2.5Sn at cryogenic temperatures is a dimpled rupture where the first voids that form are cigar-shaped and result in elongated dimples on the fracture surfaces. Fracture by such a mechanism is shown schematically in Figure 20. The schematic drawing shows the structure in three dimensions treating everything but the voids as being transparent. Figure 20a shows the first stage of the fracture process

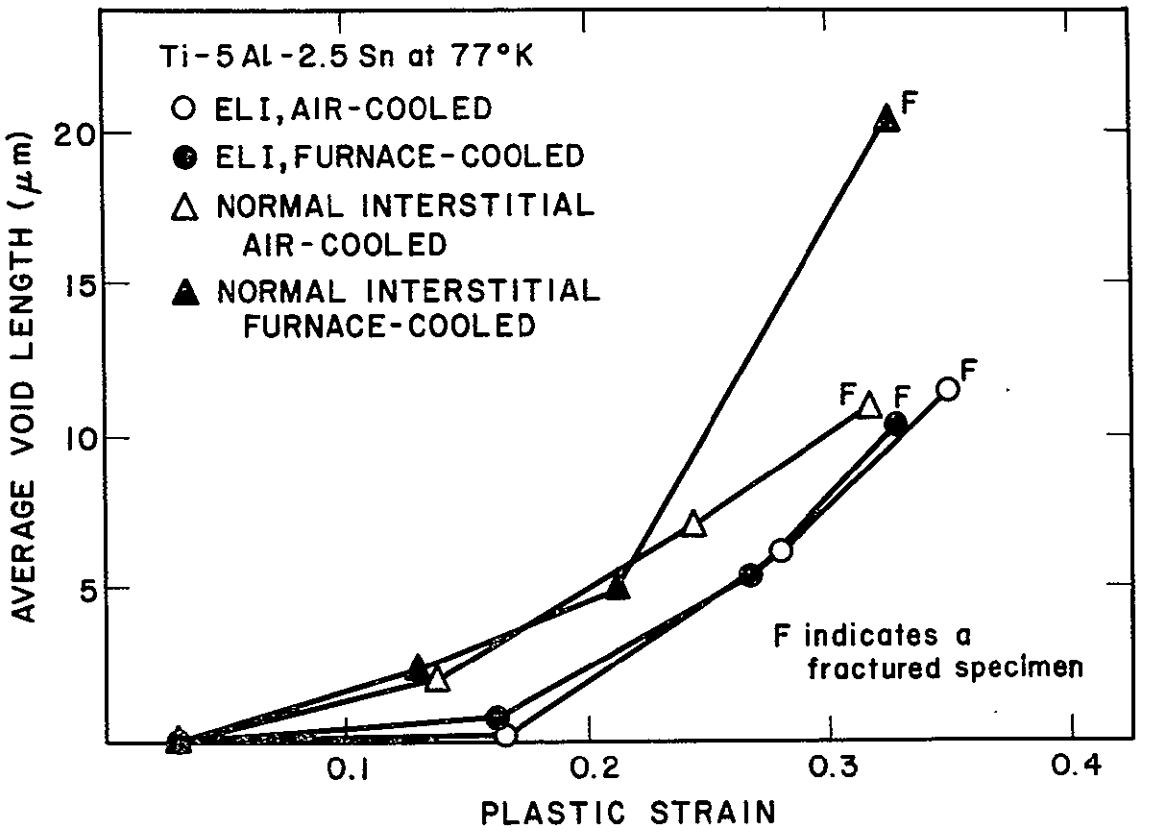

Figure 19. Variation of the Average Void Length of the Ti-5Al-2.5Sn Alloys with Plastic Strain at 77°K.

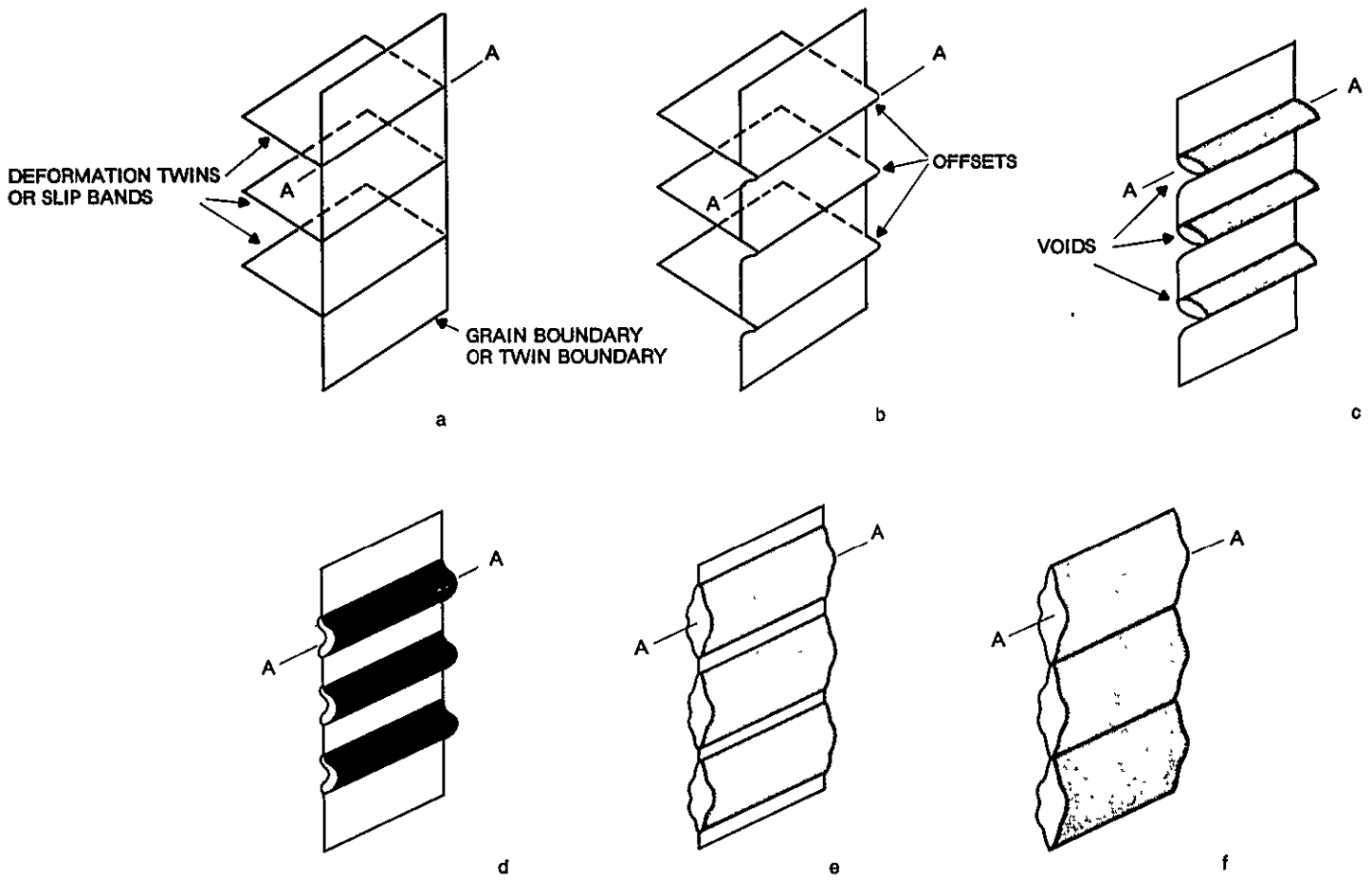

Figure 20. Schematic of the Sequence of Events During Fracture by Elongated Dimples.

where several planar slip bands or deformation twins intersect a twin or grain boundary. In this figure, the applied stress is considered to be perpendicular to the boundary; however, this is not a stringent restriction on this model. During the sectioning study, many voids were often observed along boundaries which were at large angles to the axis of applied stress. Figure 20b shows the formation of offsets in the boundary at the end of the blocked shear bands. Figure 20c shows decohesion at the offset and the void nucleation event. With larger plastic strain, the voids grow along the boundaries as shown in Figures 20d and 20e. During the void growth process, the voids spread along the boundaries more rapidly than they grow into the two adjacent crystals. Void growth occurs by plastic deformation and will tend to obliterate the sharp offsets that were present prior to void nucleation. Figure 20f shows void coalescence by the impingement of the voids. Each stage of the fracture process will be discussed separately.

Void Nucleation

The void nucleation process has two steps--the formation of offsets at the end of an intense, localized shear band and decohesion at the offset. Offset formation is controlled by the intensity of the shear band in one grain and the ability of the adjacent grain to accommodate the localized formation. For an offset nucleated by an intense slip band, offset formation will be largely controlled by the number of dislocations in the slip band. Stroh's model of a dislocation pile up[40,41,42] shows that the stress concentration factor at the end of a blocked slip band is proportional to the number of dislocations in the band. Increasing the spacing between slip bands in materials with equivalent grain sizes would increase the number of dislocations per slip band and thus enhance

offset formation. Increasing the slip band length by increases in grain size would also promote offset formation by allowing more dislocations per slip band.

For offsets nucleated by twins, the offset will be caused by the local strain of the twin. This is analogous to the dislocation approach for slip bands because the local strain in a slip band also increases with the number of dislocations. The investigation of Paton and Backofen[43] of twinning during compression of single crystals of unalloyed titanium showed that the fraction or deformation which results solely from the twinning shear increases with decreasing temperature. At room temperature, the lowest temperature studied by these investigators, more than 90 percent of the deformation resulted from the twinning shear. This suggests that at cryogenic temperatures, most of the deformation associated with twins in Ti-5Al-2.5Sn will result from the twinning shear. The localized shear in a deformation twin will be equal to the product of the twinning shear and the twin thickness. The twinning shear is determined solely by the crystallographic twinning elements; however, the twin thickness may be altered with microstructural changes. Hull[44] has shown that the thickness of twins in 3 percent silicon iron increases with increasing grain size. There is no experimental evidence on the influence of grain size on twin thickness in α titanium; but it is believed that this is a general trend.[45] If one assumes that offset nucleation will occur when the local strain reaches some critical value, it seems that a reduction in α grain size and, in turn, twin thickness will require higher macroscopic strains for offset formation and void nucleation.

The models of offset formation at the intersection of slip bands or deformation twin with a boundary suggest that if the stress and strain fields associated with these deformation modes could be reduced, offset formation

could be delayed to higher macroscopic strains. The way to accomplish this is to reduce the α grain size and to have a more even distribution of slip. The twin foil TEM of Ti-5Al-2.5 specimens deformed 3 percent in tension confirmed that this was the case. No offsets were observed in the air-cooled ELI alloy while small offsets were observed in the furnace-cooled ELI alloy. It should be noted that the higher twinning frequency will reduce the mean slip band length to some value less than the α grain size. The largest offsets occurred in the normal interstitial alloys at intersecting multiple twins. Since the total shear in a twin is proportional to the twin thickness, offset formation is more likely at the interior of a grain where lens-shaped twins are thicker. This will tend to cause a higher frequency of offset formation at twin-twin intersections than at twin-grain boundary intersections.

Offset formation is only part of the void nucleation process. At some point, it would become easier to nucleate a void than for the offset to grow larger by localized deformation systems. Using this scenario, the extent of localized deformation prior to void nucleation will be controlled by the ability of a material to accommodate an arbitrary displacement. An alloy with a more even distribution of slip could accommodate this easier than a material with more coarse slip. Metallographic sectioning experiments support this point of view. The alloys with the most uniform distribution of slip had the largest offsets while offsets in the normal interstitial alloys with their very coarse slip could only be observed using thin foil TEM.

Void nucleation was also observed at the iron-stabilized β phase of the normal interstitial alloys. Observation of spherical cavities in the troughs of the elongated dimples strongly suggest that this phase aids in the nucleation of these voids. There was no evidence that the smaller β

phase particles in the ELI alloys act as void nucleation sites. Thus, it seems that reduction of the iron content to less than that in the ELI plates (0.15 percent) would result in any further increase in fracture toughness. Broadwell and Wood[5] studied the notched properties of several ELI grade Ti-5Al-2.5Sn alloys which were doped with various levels of iron. They reported that the notched strength-to-yield ratio did not decrease until the iron content exceeded 0.2 percent. This value is consistant with the results of this investigation.

Void Growth

Serial sectioning showed that in Ti-5Al-2.5Sn, voids nucleate in the form of long tubes along offsets in boundaries. The voids then grow along the boundaries with relatively little growth into the surrounding crystals. It is generally accepted that void growth occurs by plastic deformation in the vicinity of the void. In relatively isotropic materials such as aluminum alloys[38] or steels,[32] voids retain shapes close to spheres up to the point of final fracture. In titanium, with its anisotropy and restricted number of deformation systems, it is more difficult to have homogeneous void growth. The voids in Ti-5Al-2.5Sn tend to grow along twin and grain boundaries because they can take advantage of the deformation modes available in the crystals on both sides of the boundary. To a rough approximation, twice as many deformation systems will operate for void growth along boundaries than for growth within a crystal.

Void Coalescence

Metallographic sectioning showed that void coalescence occurs by the impingement of various types of voids. If there is no interceding fracture process which aborts the growth of elongated voids, it is interesting to contemplate why approximately one-half of the fracture surfaces are covered with elongated dimples. In the early stages of the fracture

process, voids can grow across entire grains without interference from voids on other boundaries. As the void population increases, the spacing between voids will decrease to less than the α grain size, the maximum void length. The void length will then be restricted so that the new void will have lower aspect ratios. This is a volume filling restriction such as in impingement of newly recrystallized regions. Anderson and Mehl[46] noted that during the recrystallization of aluminum, impingement precluded the measurement of the growth of recrystallized regions at recrystallization volume fractions between 10 and 15 percent. Thus, it is not surprising that only half of the fracture surfaces are covered by the elongated dimples.

Of the three stages in the fracture process of Ti-5Al-2.5Sn, void nucleation is the most important. Void growth or coalescence cannot occur without first having void nucleation. Void nucleation, in effect controls the extent to which individual voids grow. Some workers[47] treat void growth as the most important stage of the dimpled rupture process because it is most likely that more energy is absorbed during void growth than either cavity nucleation or coalescence. As pointed out by Rice and Johnson,[48] the critical parameter in determining the energy absorbed during void growth is the size to which the voids grow prior to coalescence. That size will be determined by the spacing between the void nucleation sites. An increase in the number of void nucleation sites will decrease their spacing and the energy absorbed during void growth.

The fracture mechanism of Ti-5Al-2.5Sn is a good example of void growth being largely controlled by void nucleation. The widths of dimples on the fracture surface is a measure of the spacing between void nucleation sites. As was previously shown in Figure 7, the dimple width

decreased with decreasing toughness. Sectioning experiments showed that less tough alloys nucleate voids at lower strains than the toughest alloy. At equivalent macroscopic strains, more voids will have initiated in the lower toughness materials.

During the discussion of the mechanism of void nucleation, it was suggested that a reduction in α grain size would increase the macroscopic strains required for void nucleation resulting in a higher K_{Ic}. The intercept grain size of the furnace-cooled ELI alloy is approximately 25 percent larger than that of the air-cooled ELI material. The question can then be raised as to whether the source of lower toughness in the furnace-cooled ELI alloy results from ordering of larger grain size. Although it is impossible to answer that question positively, the study of deformation modes suggests that ordering played the largest role in reducing fracture toughness. In the larger grain size, ordered furnace-cooled ELI alloy, the twin volume fraction was reduced and the slip bands were spaced farther apart than in the tougher air-cooled ELI alloy. One would expect that increases in grain size would increase rather than decrease the frequency of twinning and have little effect on slip band structure. It seems then that ordering has a larger influence on the deformation modes of the ELI alloys than any grain size effects. It is the interaction of these deformation modes with boundaries that changed the frequency of void nucleation.

The furnace-cooled normal interstitial alloy was also ordered but had the same fracture toughness as the disordered air-cooled normal interstitial plate. The reason for this is that the ordering in the normal interstitial alloys caused only minor reductions in twin volume fraction and minor changes in the slip band spacing as observed in TEM. Since the fracture process is largely controlled by the deformation modes, it

is not surprisng that the two normal interstitial alloys with very similar deformation characteristics have statistically identical K_{Ic} values.

CONCLUSIONS

The fracture mechanism in Ti-5Al-2.5Sn is dimpled rupture with approximately half of the fracture surface covered by elongated dimples similar in appearance to "flutes" on stress corrosion failures in titanium and zirconium alloys. The elongated dimples nucleate as cigar-shaped voids at offsets in twin boundaries or grain boundaries caused by the intersection of intense slip bands or deformation twins with those boundaries. The cigar-shaped voids grow along the boundaries with relatively little growth into the crystals on either side of the boundary. Voids also nucleate at the iron-stabilized β phase particles. This type of void nucleation can be essentially eliminated by reducing the particle size through reduction in the iron content to 0.15 percent. Void coalescence occurs by impingement of the cigar-shaped and β-nucleated voids.

The fracture toughness of Ti-5Al-2.5Sn at cryogenic temperatures is controlled by the number of void nucleation events which in turn effects the extent to which voids grow. Any compositional change which promotes a more uniform distribution of deformation will improve the fracture toughness. K_{Ic} can be increased by having the lowest possible interstitial level, cooling rapidly from the annealing temperature so as to avoid ordering, and by reducing the iron content to below 0.15 percent. It was also suggested that reductions in α grain size would improve toughness in Ti-5Al-2.5Sn at cryogenic temperatures.

ACKNOWLEDGMENTS

This work was performed under National Aeronautics and Space Administration Grant NGR-39-087-047. The authors would like to thank

W. F. Brown, Jr. and W. D. Klopp of that organization for their helpful support and comments. I. Mella also provided excellent experimental assistance during the thin foil TEM study of the deformed specimens. Finally, the authors wish to express their gratitude to Mrs. Jean Ballew who was of invaluable assistance throughout the course of this work and in the preparation of this manuscript.

REFERENCES

1. J. L. Shannon, Jr. and W. F. Brown, Jr., Proc. ASTM, 63, 1963, p. 809.
2. R. E. Curtis, R. R. Boyer, and J. C. Williams, Trans. ASM, 62, 1969, p. 457.
3. Anthony W. Thompson and Ben C. Odegard, Met. Trans., 4, 1973, p. 899.
4. J. L. Christian, A. Hurlich, J. E. Chafey, and J. F. Watson, Proc. ASTM, 63, 1963, p. 578.
5. R. G. Broadwell and R. A. Wood, Materials Research and Standards, 4, 1964, p. 549.
6. M. J. Blackburn, Trans. AIME, 239, 1967, p. 1200.
7. T. K. G. Namboodhiri, C. J. McMahon, Jr., and H. Herman, Met. Trans., 4, 1973, p. 1323.
8. Paul Pietrokowsky and Ellis P. Frink, Trans. ASM, 49, 1957, p. 339.
9. J. C. Williams and M. J. Blackburn, Ordered Alloys, Structural Applications and Physical Metallurgy, Claitors, Baton Rouge, 1970, p. 425.
10. N. E. Paton, J. C. Williams, and G. P. Rauscher, Titanium Science and Technology, Plenum Press, New York, 1973, p. 1049.
11. N. E. Paton, R. G. Baggerly, and J. C. Williams, "Deformation and Solid Solution Strengthening of Titanium Aluminum Single Crystals," Report SC 526.7FR, Rockwell International Science Center, January 20, 1976.
12. A. M. Garde, E. Aigeltinger, and R. E. Reed-Hill, Met. Trans., 4, 1973, p. 2461.
13. M. J. Blackburn, Trans. ASM, 59, 1966, p. 694.
14. M. G. Mendiratta, Amiya A. Chakrabarti, and J. A. Roberson, Met. Trans., 5, 1974, p. 1949.
15. Titanium Alloys Handbook, MCIC-HB-02, Metals and Ceramics Information Center, Battelle Columbus Laboratories, December 1972.
16. J. C. Williams, R. R. Boyer, and M. J. Blackburn, ASTM STP 453, 1969, p. 215.

17. C. J. Beevers and D. V. Edmonds, Trans. AIME, 245, 1969, p. 2391.

18. M. F. Amateau, H. I. Burrier, Jr., and L. J. Ebert, Trans. ASM, 59, 1966, p. 920.

19. M. F. Amateau and E. A. Steigerwald, "The Relationship between Plastic Deformation and Fracture in Alpha Titanium," AFML-TR-66-263, June 1966.

20. H. W. Worner, J. Inst. of Metals, 79, 1951, p. 173.

21. M. J. Blackburn and J. C. Williams, Trans. AIME, 239, 1967, p. 287.

22. B. W. Levinger, Trans. AIME, 197, 1953, p. 195.

23. S. K. Das and G. Thomas, Order-Disorder-Transformations in Alloys, Springer-Verlag, Berlin, 1974, p. 332.

24. R. H. Olsen, Metallography, 5, 1972, p. 369.

25. R. H. Van Stone, J. L. Shannon, Jr., W. S. Pierce, and J. R. Low, Jr., "The Influence of Composition, Annealing Treatment, and Texture on the Fracture Toughness of Ti-5Al-2.5Sn at Cryogenic Temperatures," to be published.

26. "Standard Method of Test for Plane-Strain Fracture Toughness of Metallic Materials," ASTM Designation E399-74.

27. H. Conrad, K. Okasaki, V. Gadgil, and M. Jon, Electron Microscopy and Structure of Materials, University of California Press, Berkeley, 1972, p. 438.

28. G. Sanderson and J. C. Scully, Corrosion Science, 8, 1968, p. 541.

29. R. J. H. Wanhill and P. deRisk, Brit. Corr. J., 9, 1974, p. 84.

30. I. Aitchison and B. Cox, Corrosion, 28, 1972, p. 83.

31. S. Mahajan, Phil. Mag., 23, 1971, p. 781.

32. T. B. Cox and J. R. Low, Jr., Met. Trans., 5, 1974, p. 1457.

33. R. H. Van Stone and J. A. Psioda, Met. Trans., 6A, 1975, p. 668.

34. H. C. Rogers, Trans. AIME, 218, 1960, p. 498.

35. R. E. Reed-Hill, Deformation Twinning, Gordon & Breach, New York, 1964, p. 295.

36. N. S. Stoloff and R. G. Davies, Trans. ASM, 57, 1964, p. 247.

37. N. S. Stoloff and R. G. Davies, Prog. Mat. Sci., 13, 1966, p. 3.

38. R. H. Van Stone, R. H. Merchant, and J. R. Low, Jr., ASTM STP 556, 1974, p. 93.

39. M. A. Greenfield and H. Margolin, Met. Trans., 3, 1972, p. 2649.

40. A. N. Stroh, Proc. Roy. Soc., A223, 1954, p. 404.

41. A. N. Stroh, Proc. Roy. Soc., A233, 1955, p. 548.

42. A. N. Stroh, Adv. in Physics, 6, 1957, p. 418.

43. N. E. Paton and W. A. Backofen, Met. Trans., 1, 1970, p. 2839.

44. D. Hull, Acta Met., 9, 1961, p. 191.

45. S. Mahajan and D. F. Williams, Met. Rev., 18, 1973, p. 43.

46. W. A. Anderson and R. F. Mehl, Trans. AIME, 161, 1945, p. 140.

47. G. T. Hahn and A. R. Rosenfield, Met. Trans., 6A, 1975, p. 653.

48. James R. Rice and M. Arthur Johnson, "The Role of Large Crack Tip Geometry Changes in Plane Strain Fracture," presented at the Battelle Colloquium on Inelastic Behavior of Solids, Columbus and Atwood Lake, Ohio, September 1969.

PART II

THE INFLUENCE OF COMPOSITION, ANNEALING TREATMENT, AND TEXTURE ON THE FRACTURE TOUGHNESS OF Ti-5Al-2.5Sn AT CRYOGENIC TEMPERATURES

INTRODUCTION

Titanium alloys are used in a wide variety of aerospace structures due to their high strength-to-density ratio. Equally important to the structural reliability of these vehicles is a high fracture toughness. This paper will describe a portion of an investigation on the influence of microstructure on the fracture toughness of Ti-5Al-2.5Sn at cryogenic temperatures. Ti-5Al-2.5Sn is an α titanium alloy which has often been used for the storage tanks and pumping systems for liquid hydrogen in applications such as manned spacecraft. Similar light weight tankage may also be a prerequisite for new technologies such as the evolution of a hydrogen economy. This paper will describe the variations in smooth tensile properties and plane strain fracture toughness (K_{Ic}) with test temperature, interstitial level, cooling rate from the annealing temperature, and specimen orientation. The source of some of these variations have been discussed elsewhere and will be summarized in this paper.

BACKGROUND

During the early 1960's, several investigations determined the mechanical properties of Ti-5Al-2.5Sn sheet at cryogenic temperatures. These investigations preceded the widespread use of linear elastic fracture mechanics, so notched tensile specimens were used to assess toughness. Christian, et al.[1] studied the smooth and notched tensile properties of Ti-5Al-2.5Sn sheet which was annealed at 788°C (1450°F) and evaluated at the temperature of liquid nitrogen (77°K or -320°F) or liquid hydrogen (20°K or -423°F). As is typical for titanium alloys, increases in oxygen content resulted in higher tensile strength, lower tensile ductility, and lower notched-to-unnotched strength ratios. The strength ratios dropped sharply in alloys with oxygen contents in excess of 0.10 percent. They also noted

that two alloys with iron contents greater than 0.25 percent had lower notched tensile strengths than those determined for alloys with lower iron contents and similar oxygen levels. Broadwell and Wood[2] showed that the notched strength-to-yield ratios for Ti-5Al-2.5Sn alloys with oxygen contents less than 0.12 percent dropped suddenly when the iron content exceeded 0.2 percent.

As a result of these types of investigations, two grades of Ti-5Al-2.5Sn became common - extra low interstitial (ELI) for applications requiring high toughness and normal interstitial. ELI grades have oxygen contents less than 0.12 percent and iron contents between 0.1 and 0.2 percent. Normal interstitial grades have oxygen and iron contents less than 0.2 and 0.5 percent, respectively. It is important to note that although the alloy purity is classified by the interstitial level, increased iron concentrations accompany higher interstitial levels. This is important because iron is a very strong β phase stabilizing element.[3]

Shannon and Brown[4] investigated the effect of several production and fabrication variables on smooth and notched tensile properties of ELI and normal interstitial grades of Ti-5Al-2.5Sn sheet which was mill annealed at 815°C (1500°F). At 20°K, the notched strength-to-yield strength ratio for the normal interstitial alloy is about 50 percent less than the ratio of the ELI alloy. This clearly illustrates the inferior toughness of the lower purity material. These investigators also studied the influence of cooling rate from the 815°C annealing temperature on the properties of the ELI sheet material. At 20°K, air-cooled and furnace-cooled sheet had essentially identical smooth tensile properties; but the notched strength of the furnace-cooled material was about 25 percent below that of the air-cooled material. The lower notched strength in the furnace-cooled sheet was attributed to precipitation of the ordered α_2 phase which occurs in titanium-aluminum alloys;[5, 6] however, no attempt was made to experimentally observe α_2.

With the development of linear elastic fracture mechanics, an ASTM standard test method for determining the plane strain fracture toughness (K_{Ic}) was developed.[7] Several investigators attempted to measure K_{Ic} in Ti-5Al-2.5Sn; but due to the thickness restrictions of the ASTM standard, much of this data is invalid. In this paper, invalid K_{Ic} data will be referred to as K_Q. Curtis, Boyer, and Williams[8] studied the effect of post-anneal aging on the room temperature toughness of normal interstitial Ti-5Al-2.5Sn plate which was air-cooled after a 760°C (1400°F) annealing treatment. Portions of this plate were step cooled at 593°C (1100°F) and 500°C (932°F). Both annealed and aged plate had similar yield strengths. K_Q at room temperature was 79MN-$m^{-3/2}$ (72 ksi/in.) for the annealed plate but only 51MN-$m^{-3/2}$ (46 ksi/in.) in the aged material. Electron diffraction of the aged plate did not reveal any evidence of α_2 precipitation. The results of Curtis, et al.[8] are consistent with those of Shannon and Brown[4] in that slow cooling or aging reduces the toughness of Ti-5Al-2.5Sn.

Several other investigations have measured K_Q and K_{Ic} in annealed Ti-5Al-2.5Sn forgings at cryogenic temperatures. The cooling rate from the annealing temperature is not known for these forgings. At 20°K, their K_{Ic} values range from 59MN-$m^{-3/2}$ (53 ksi/in.) to 92MN-$m^{-3/2}$ (83 ksi/in.).[9,10] To date, no investigation had determined valid K_{Ic} values at cryogenic temperatures for a variety of compositional and heat treatment variables, even though this alloy was used for liquid hydrogen storage vessels in the American space program. It is hoped that this investigation will provide a portion of this required data base.

EXPERIMENTAL APPROACH

The purpose of this investigation is to determine the influence of test temperature, alloy purity, cooling rate from annealing temperature, and

specimen orientation on the fracture toughness of Ti-5Al-2.5Sn. Obviously, not all aspects of these areas can be addressed in a single investigation. The approach taken here is very similar to that of Shannon and Brown.[4]

The mechanical properties and fracture mechanisms were studied in commercially produced ELI and normal interstitial plates. Portions of each plate were either air-cooled or furnace-cooled from the annealing temperature. Tensile and fracture toughness tests were performed at room temperature (295°K), liquid nitrogen temperature (77°K), and liquid hydrogen temperature (20°K). The microstructure of these plates has been characterized and the fracture mechanism has been studied with fractography and metallographic sectioning studies. These results have been reported in detail elsewhere[11] and will be summarized here to explain the trends in fracture toughness.

MATERIALS

Ti-5Al-2.5Sn is being investigated in ELI and normal interstitial grade alloys which were either air-cooled or furnace-cooled from an 815°C (1500°F) mill annealing treatment. Plate material, 25mm (1 inch) thick was fabricated and heat treated by a commercial vendor. The air-cooled and furnace-cooled plates were processed from the same heat to avoid minor variations in composition. The compositional specification, heat analyses, and check analyses of these plates are given in Table I. In the normal interstitial plates, the iron content is approximately two times greater and the oxygen levels are about three times larger than those of the ELI alloy.

The furnace-cooling rate is approximately 15C° (27F°) per hour. The initial air-cooling rate is about 4500C° (8100F°) per hour and it took the plate about an hour to reach room temperature.

TABLE I

CHEMICAL ANALYSES OF Ti - 5 Al - 2.5 Sn ALLOYS
(Weight Percent)

	Al	Sn	Fe	Mn	O	C	N	H
Normal Int. Specification	4.0/6.0	2.0/3.0	0.50 Max	0.30 Max	0.20 Max	0.15 Max	0.07 Max	0.003/0.020
Normal Int. Heat Analysis	5.1	2.5	0.28	0.006	0.16	0.024	0.023	0.009
Normal Int., AC* Check Analysis	5.22	2.47	0.300	0.002	0.164	0.0140	0.0163	0.0072
Normal Int., FC† Check Analysis	5.24	2.47	0.270	0.002	0.169	0.0120	0.0172	0.0042
ELI Specification	4.7/5.6	2.0/3.0	0.1/0.2	--	0.12 Max	0.08 Max	0.05 Max	0.0125 Max
ELI Heat Analysis	5.0	2.6	0.16	0.006	0.086	0.023	0.010	0.006
ELI, AC * Check Analysis	5.09	2.44	0.140	0.002	0.054	0.0057	0.0098	0.0056
ELI, FC † Check Analysis	5.10	2.47	0.145	0.002	0.052	0.0041	0.0098	0.0050
Maximum Error in Check Analysis	0.200	0.150	0.010	0.0005	0.010	0.0010	0.0010	0.0010

* Air Cooled
† Furnace Cooled

The microstructure of these plates was studied using optical metallography, thin foil transmission electron microscopy (TEM), microprobe analysis, and texture pole figures. These results have been reported elsewhere and are summarized in Table II. The plates had equiaxed α grains. The α grain sizes are similar in all the plates except the furnace-cooled ELI plate where the grain size is slightly larger.

The alloy purity as indicated by the interstitial level affected the dispersion of the iron-stabilized β phase and crystallographic texture. The normal interstitial alloys with their higher iron content had larger β particle size and volume fraction of the iron-stabilized β phase than the ELI material. The ELI plates had an α annealing texture where the normal interstitial alloys have a β deformation texture. Figure 1 shows a computer plotted pole figure of the basal (0002) and prism ($10\bar{1}0$) planes for the air-cooled ELI plate. This texture is a typical α annealing texture where the basal planes are parallel to the plate surface. Figure 2 shows the pole figures for the air-cooled normal interstitial plate. This is a β processing texture where the basal planes are perpendicular to the longitudinal and transverse directions. The maximum basal texture is only four times random intensity which is quite mild for titanium alloys. Figures 1 and 2 show that the prism planes are distributed in an almost random intensity. Although both plates were to have been processed identically, these differences in texture suggest that the processing was quite different. Variation in cooling rate did not greatly affect the texture pole figures.

Changes in cooling rate altered the ordering characteristics of the α matrix. Superlattice reflections of the α_2 phase observed in TEM diffraction patterns of thin foils of both furnace-cooled plates. The superlattice reflections were not observed in diffraction patterns of the air-cooled alloys. The furnace-cooling rate was apparently slow enough to allow time

TABLE II

Summary of Microstructure in Ti-5Al-2.5Sn Plates

Microstructural Feature	ELI		Normal Interstitial	
	AC*	FC†	AC*	FC†
α Grain Size (μm)	46.2	58.1	41.6	41.4
Estimated Size of Iron-Stabilized β Particles (μm)	2	2	5	5
α Precipitation within β	?	No	Yes	No
Ordering	No	Yes	No	Yes
Type of Texture	α	α	β	β

* AC indicates air-cooled.

† FC indicates furnace-cooled.

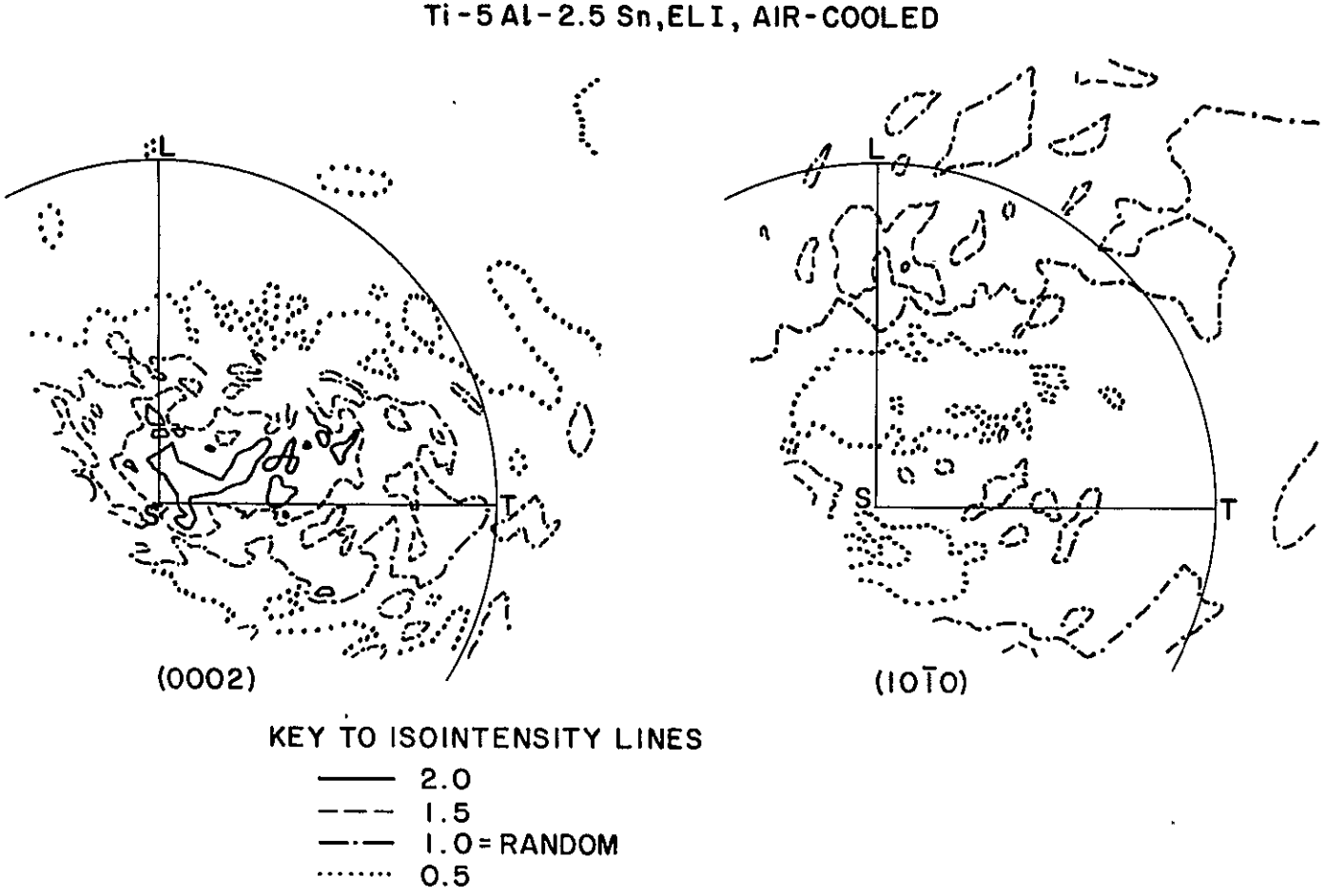

Figure 1. Texture Pole Figure of Air-Cooled ELI Ti-5Al-2.5Sn Plate. L, T, and S indicate longitudinal, transverse, and short transverse directions, respectively.

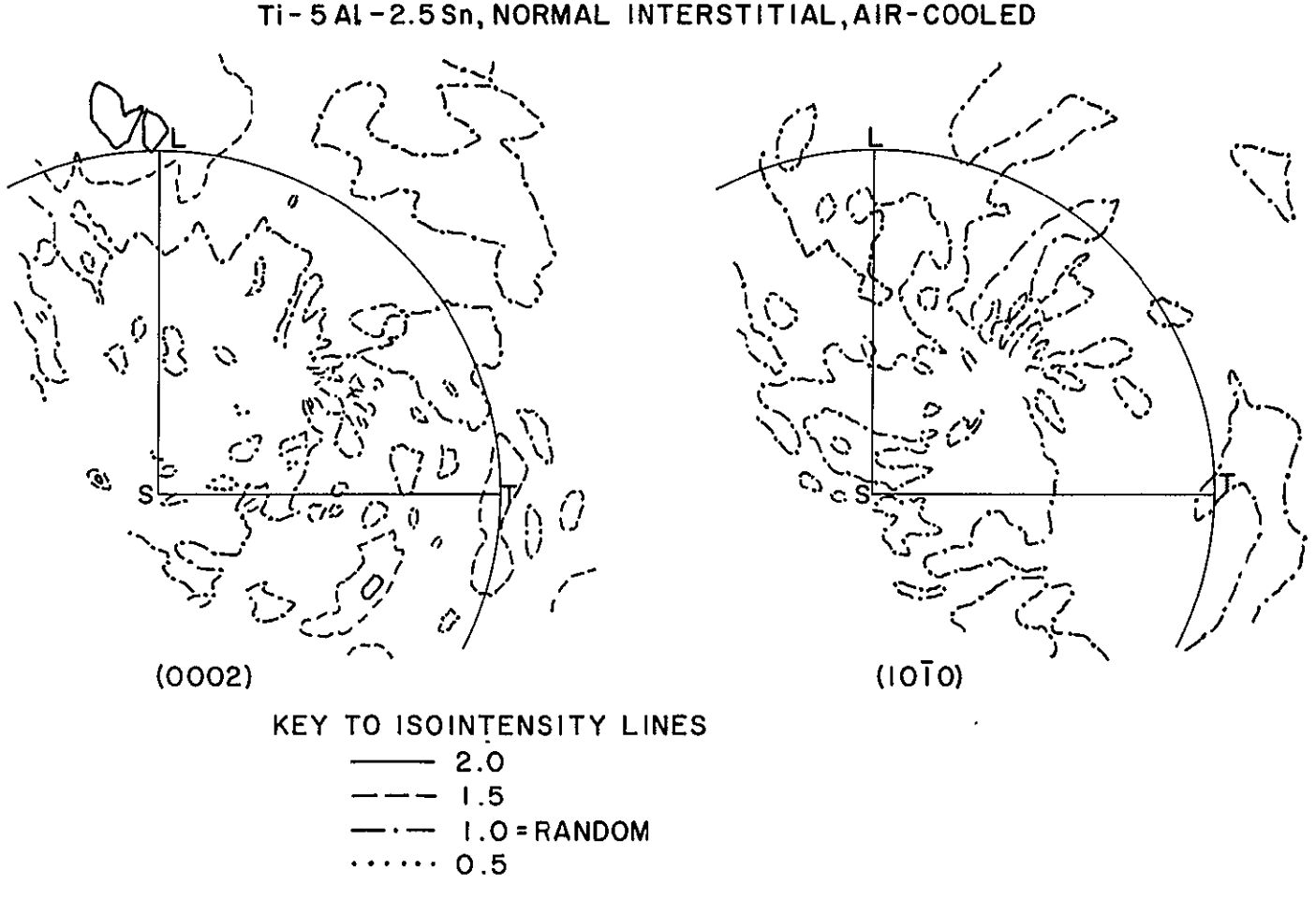

Figure 2. Texture Pole Figure of Air-Cooled Normal Interstitial Ti-5Al-2.5Sn Plate. L, T, and S indicate longitudinal, transverse, and short transverse directions, respectively.

for the sluggish ordering transformation[5, 6] to occur. Furnace-cooled alloys will be considered to be ordered while the air-cooled alloys will be referred to as disordered alloys.

MECHANICAL PROPERTIES

The tensile properties and plane-strain fracture toughness (K_{Ic}) of the Ti-5Al-2.5Sn alloys were determined at 20°K, 77°K, and 295°K.* The 77°K tests were conducted in a foam insulated, strainless steel dewar filled with liquid nitrogen which was part of the load strain in 0.27 MN (60 Kip) universal testing machine. The 20°K specimens were totally immersed in liquid hydrogen in super-insulated vacuum-jacketed cryostats and loaded in either a 0.53 MN (120 Kip) or a 178 MN (400 Kip) hydraulic universal testing machine. Liquid level was sensed using carbon resistor probes. The construction, safety features, and capabilities of the liquid hydrogen testing facility have been described by Shannon, et al.[12] The specimens and techniques used in each facility are different and will be described separately.

In the tests performed at 295°K and 77°K, the specimen displacements were measured using linear variable differential transducers (LVDT). The method used to calibrate the LVDT was developed by Shannon and Pierce.[13] The output from an LVDT for a given displacement is controlled by the phase angle between the primary and secondary signal and the gain control. Ordinairly, the phase control is set to maximize the output; but in this study, the phase angle was set so that the calibrations at 295°K and 77°K were identical. The LVDT can then be calibrated at room temperature for a cryogenic test. The LVDT used in this investigation has a linear range of plus or minus 2.5 mm (0.1 inch) so that by properly setting the null point and using full-

*The mechanical properties at 77°K and 295°K were determined at Carnegie-Mellon University while the properties at 20°K were measured at the NASA-Lewis Research Center.

scale zero suppression electronics, the LVDT has a linear range of 5 mm (0.2 inch).

The tensile specimens used at 77°K and 295°K had a cylindrical gage section with a nominal diameter of 6.4 mm (0.25 inch). An LVDT extensometer with a 25.4 mm (1 inch) gage length and capable of 15 percent extension was used to record the specimen elongation. Load and elongation were autographically recorded up to the maximum load. Beyond the maximum load, the specimens were deformed slightly beyond the previous strain and unloaded. The load prior to unloading was noted and the minimum specimen diameter was measured with a point micrometer. This process was repeated several times before fracture occurred. For tests conducted in liquid nitrogen, the specimens were strained in the liquid nitrogen cryostat, removed from the cryostat, and allowed to warm to room temperature before the minimum diameter was measured. The specimens were cooled to 77°K before they were strained again.

The load-extensometer traces were used to determine the 0.2 percent offset yield strength (σ_y) and the ultimate tensile strength (UTS). The fracture strain (ε_f) was calculated from the minimum diameter of the fractured specimen. The measure of strain used throughout this report is the diametral strain (ε) as defined in Equation (1).

$$\varepsilon = 2 \ln (d_o/d) \tag{1}$$

where d_o = initial specimen diameter
and d = instantaneous specimen diameter.

The load-extensometer traces and the data taken from the point of maximum load were used to determine a true stress-plastic strain curve using standard corrections. As noted by Bridgman,[14] there is a region of hydrostatic tension in the neck of a tensile specimen. If a flow curve is

to represent the flow characteristics of the material being tested, the hydrostatic component must be subtracted from the measured axial stress. Bridgman developed an expression to perform this operation. The flow stress (σ) is calculated by multiplying the true stress by the Bridgman correction factor for cylindrical specimens, which is given in Equation (2).

$$F = 1 \; / \; \{ \; (1 + 2\,R/a) \; \ell n \; (1 + a/2R) \; \} \qquad (2)$$

where a = a minimum radius of the necked region

and R = radius of curvature of the neck.

The Bridgman correction factor is a function only of the neck geometry. Bridgman showed that a plot of a/R versus strain was linear up to strains of unity for a wide variety of steels, but there is no reason why this emperical correlation for steels should be applicable to titanium alloys. For this reason, a/R was determined for several Ti-5Al-2.5Sn alloys strained at room temperature. The a/R value was determined by placing a necked specimen on a shadowgraph with a magnification of twenty and tracing the observed neck on a piece of tracing paper. The radius of curvature was measured from a geometric construction at the neck and a was measured from the minimum diameter observed on the tracing paper. Figure 3 shows a/R plotted as a function of plastic strain for room temperature deformation of the air-cooled Ti-5Al-2.5Sn alloys and Bridgman's data for steels.[14] Also shown in the figure is the line constructed by Bridgman for steels and linear least square regression analysis for the titanium data. Although the scatter for both materials is quite wide, it is apparent that the a/R ratios for Ti-5Al-2.5Sn alloys are less than those of steels at the same strain. The a/R values for Ti-5Al-2.5Sn shown in Figure 3 were determined at 295°K. No data were taken at lower temperatures, but it is expected that

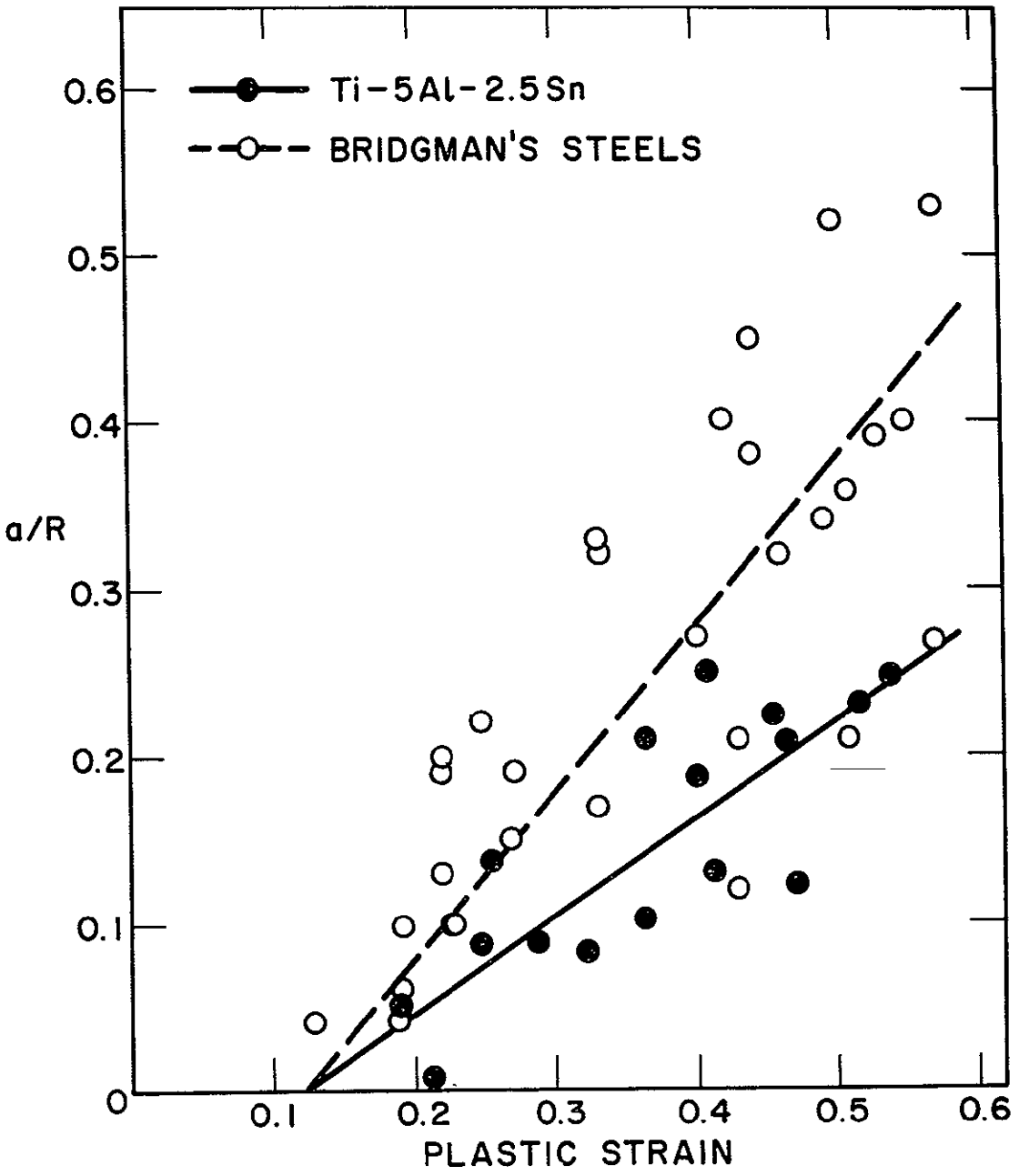

Figure 3. a/R às a Function of Plastic Strain for Ti-5Al-2.5Sn and Steels at Room Temperature.

temperature would not greatly affect a/R values. The equation for the titanium data is given in Equation (3).

$$a/R = - 0.072 + 0.589\ \varepsilon \quad . \tag{3}$$

According to this relationship, a/R would be negative at strain less than 0.122. This is the region of uniform plastic strain where no necking has occurred, so that true stress is considered to be the flow stress. Above strains of 0.122, Equations (2) and (3) are used to calculate the Bridgman correction factor and, in turn, the flow stress.

A computer program has been used to calculate the plastic strain, engineering stress, true stress, and flow stress from the load, extension, and minimum diameter data. This program also performed at least squares regression analysis on the flow stress data and fitted to the empirical flow curve of the form given in Equation (4).

$$\sigma = \sigma_o + A\ \varepsilon^m \tag{4}$$

where σ_o, A, and m are constants determined by the regression analysis. Monteiro and Reed-Hill[15] have shown that flow curve data of unalloyed titanium fits Equation (4) better than the more traditional flow curve where σ_o is assumed to be zero.

The plane strain fracture toughness tests performed at 295°K and 77°K used standard 25.4 mm (1 inch) thick compact tension specimens which are described in the ASTM Standard Test Method E399-74.[7] The displacement at the mouth of the machined notch was measured with a spring-loaded LVDT clip gage seated in knife edges attached to the specimen. This clip gage is similar to the one designed by Shannon.[13] All the features of this test facility meet the requirements of the ASTM Standard Test Method for plane strain fracture toughness testing.[7]

The 20°K tensile specimens have a circular cross-section with a nominal diameter of 11.4 mm (0.45 inch). Strain was measured using two foil-type resistance strain gages mounted on the center portion of the specimen gage length 180° apart. The strain gages were calibrated in liquid hydrogen to an accuracy within one percent. Load and strain were recorded on an X-X-Y' recorder with the output of each strain gage fed into a separate pen. The test record was used for determination of the Young's modulus and the 0.2 percent offset yield strength. The strain gages usually failed shortly after the 0.2 percent offset strain was reached. No load-time record was maintained during the remainder of the test. The maximum load and the load at which the specimen ruptured was read from the load dial of the testing machine. The information from the load-extension curve, the fracture load, and the minimum diameter of the fractured specimen was used in the computer program previously described to determine the constants of the empirical flow curve given in Equation (4).

Two sizes of three-point bend plane-strain fracture toughness specimens were used to determine K_{Ic} at 20°K. They were 25.4 mm (1 inch) thick by either 25 mm (1 inch) or 50 mm (2 inch) in width and will be referred to as 1x1 and 1x2 bend specimens, respectively, throughout the balance of this paper. Both of these specimen designs are recommended in the ASTM test method.[7] Crack mouth opening was sensed using a double cantilever beam clip-in gage of the type described in ASTM Standard Test Method E-399. The displacement was measured with strain gages mounted on the arms of the clip gage using low excitation voltage to prevent heating of the gages and consequent boiling of the liquid hydrogen and agitation of the gage arms. Gage linearity, in liquid hydrogen, was within 0.0001 inch over the calibrated range from 5 mm (0.2 inch) to 6.5 mm (0.25 inch) and was accurate within 1 percent. Full details of

the load fixturing, instrumentation, and test procedures are described by Shannon, et al.[12] This test facility conformed to the requirements of ASTM Standard Method E-399 for Plane-Strain Fracture Toughness of Metallic Materials.

The conventional tensile properties were determined with specimens in the longitudinal orientations. The plane strain fracture toughness at 295°K and 77°K was determined using 25 mm (1 inch) thick compact tension specimens in the LT orientation (the fracture surface is perpendicular to the longitudinal direction and the crack propagates in the transverse direction). At 20°K, the plane strain fracture toughness was determined for the LS (the fracture surface is perpendicular to the longitudinal direction and the crack propagates in the short transverse direction) and LT orientations. At 20°K, the LT orientation K_{Ic} was determined using both 1x1 and 1x2 bend specimens, while 1x1 bend specimens were used to measure the LS fracture toughness. The maximum stress in all the specimens is parallel to the longitudinal directions. The LS specimens were included for comparison with 20°K longitudinal surface crack specimen results which have been obtained at NASA Lewis Research Center using the same Ti-5Al-2.5Sn plates as this investigation. The 25 mm (1 inch) width of the 1x1 LS specimens was limited by the plate thickness. The two specimen sizes tested in the LT orientation at 20°K were intended to explore the influence of specimen size on K_{Ic}. This comparison will be used to determine if the results from 1x1 LS specimens can be compared with those from 1x1 LT specimens. Such comparisons would permit identification of the variation of toughness with crack orientation in the plate.

During the investigation, 17 percent of the fracture toughness tests should be considered invalid based on the ASTM criteria for fatigue crack front curvature.[7] According to E-399, a K_Q value is invalid if the crack

length at the center of the specimen and at positions halfway between the center and edge of the specimen deviate from the average of these three crack lengths by more than 5 percent. A statistical analysis was performed to show that this criteria could be relaxed to 10 percent without increasing the scatter in K_{Ic} data. Kaufman and Cordier[16] conducted an extensive analysis of crack front curvature effects in aluminum alloys and reached the same conclusion. As a result of these analyses, K_{Ic} values reported as valid data in this paper will include results from specimens with crack front curvatures less than 10 percent.

The tensile and fracture toughness properties of the Ti-5Al-2.5Sn alloys are given in Table III. These data represent the average and standard deviation of multiple tests except where otherwise noted.

Figure 4 shows the longitudinal strength and LT orientation fracture toughness for the Ti-5Al-2.5Sn alloy as a function of testing temperature. The 20°K K_{Ic} data shown is from the results of the 1x2 bend specimens. The error bars indicate the range of plus and minus one standard deviation (68 percent confidence limits). If no error bar is shown, the standard deviation is smaller than the point representing the average value. The room temperature fracture toughness data of the ELI alloys as shown in Figure 4 are invalid and represent the results of single tests.

The strength level of the normal interstitial alloys are about 175 MN/m^2 (25 ksi) higher than the ELI alloys. For both grades, the yield strength at 20°K is approximately twice that of room temperature. In most cases, the ultimate tensile strength is about 70 MN/m^2 (10 ksi) higher than the yield strength. Both the yield strength and ultimate tensile strength decrease in a linear fashion with increasing testing temperature. As in the investigation of Shannon and Brown,[4] variations in cooling rate did not affect the smooth tensile properties.

TABLE III

Mechanical Properties of Ti-5Al-2.5Sn Plates

(Data indicates the mean ± one standard deviation)

Alloy	Test Temperature °K (°F)	σ_y 0.2% Yield Strength (ksi) (a)	Ultimate Tensile Strength (ksi) (a)	Tensile Fracture Strain	K_{Ic} (ksi√in.) (b)	K_{Ic} Specimen Orientation (f) and Type
Ti-5Al-2.5Sn	295 (72)	102.1 ± 0.8	110.2 ± 1.1	0.528 ± 0.012	107.9 (c, d, g)	LT-CT (e)
ELI	77 (-320)	171.4 ± 2.0	181.9 ± 0.6	0.407 ± 0.041	101.1 ± 4.4	LT-CT
Air-Cooled	20 (-423)	189.0 ± 1.0	203.5 ± 0.8	0.254 ± 0.028	81.5 ± 4.5	LT-1x2 Bend
					82.7 ± 1.8	LT-1x1 Bend
					96.9 ± 4.5(g)	LS-1x1 Bend
Ti-5Al-2.5Sn	295 (72)	98.9 ± 0.7	108.4 ± 0.4	0.512 ± 0.025	104.9 (c, g)	LT-CT
ELI	77 (-320)	170.6 ± 0.5	180.5 ± 1.0	0.402 ± 0.024	75.1 ± 0.4	LT-CT
Furnace-Cooled	20 (-423)	189.4 ± 0.3	204.7 ± 1.6	0.207 ± 0.043	64.0 ± 1.1	LT-1x2 Bend
					61.8 ± 2.2	LT-1x1 Bend
					73.4 ± 5.1	LS-1x1 Bend
Ti-5Al-2.5Sn	295 (72)	126.9 ± 0.5	133.8 ± 0.4	0.435 ± 0.040	65.4 ± 4.4	LT-CT
Normal Interstitial	77 (-320)	194.5 ± 1.0	207.3 ± 1.1	0.317 ± 0.015	48.6 ± 1.3	LT-CT
Air-Cooled	20 (-423)	215.4 ± 2.3	228.9 ± 0.1	0.209 ± 0.029	46.8 ± 1.0	LT-1x2 Bend
					46.0 ± 1.0 (h)	LT-1x1 Bend
					45.7 ± 0.4	LS-1x1 Bend
Ti-5Al-2.5Sn	295 (72)	127.9 ± 0.6	132.6 ± 0.6	0.328 ± 0.055	60.0 ± 1.3	LT-CT
Normal Interstitial	77 (-320)	200.0 ± 0.5	209.9 ± 0.3	0.327 ± 0.034	52.5 ± 1.8	LT-CT
Furnace-Cooled	20 (-423)	220.3 ± 1.2	228.7 ± 0.4	0.124 ± 0.051	46.2 ± 0.2	LT-1x2 Bend
					42.7 ± 0.3	LT-1x1 Bend
					47.8 ± 3.3	LS-1x1 Bend

(a) 1 ksi = 6.9 MN/m^2

(b) 1 ksi√in = 1.1 $MN/m^{3/2}$

(c) This result is invalid because specimen thickness is less than 2.5 $(K_{Ic}/\sigma_y)^2$. Only one test was conducted.

(d) This result is invalid because the maximum load exceeded the 5% tangent load by more than 10%.

(e) CT indicates a compact tension specimen.

(f) Orientation notation is that of ASTM E399-74.

(g) This result is invalid because crack length is less than 2.5 $(K_{Ic}/\sigma_y)^2$.

(h) This result is invalid because the crack length-to-specimen width is in excess of 0.55.

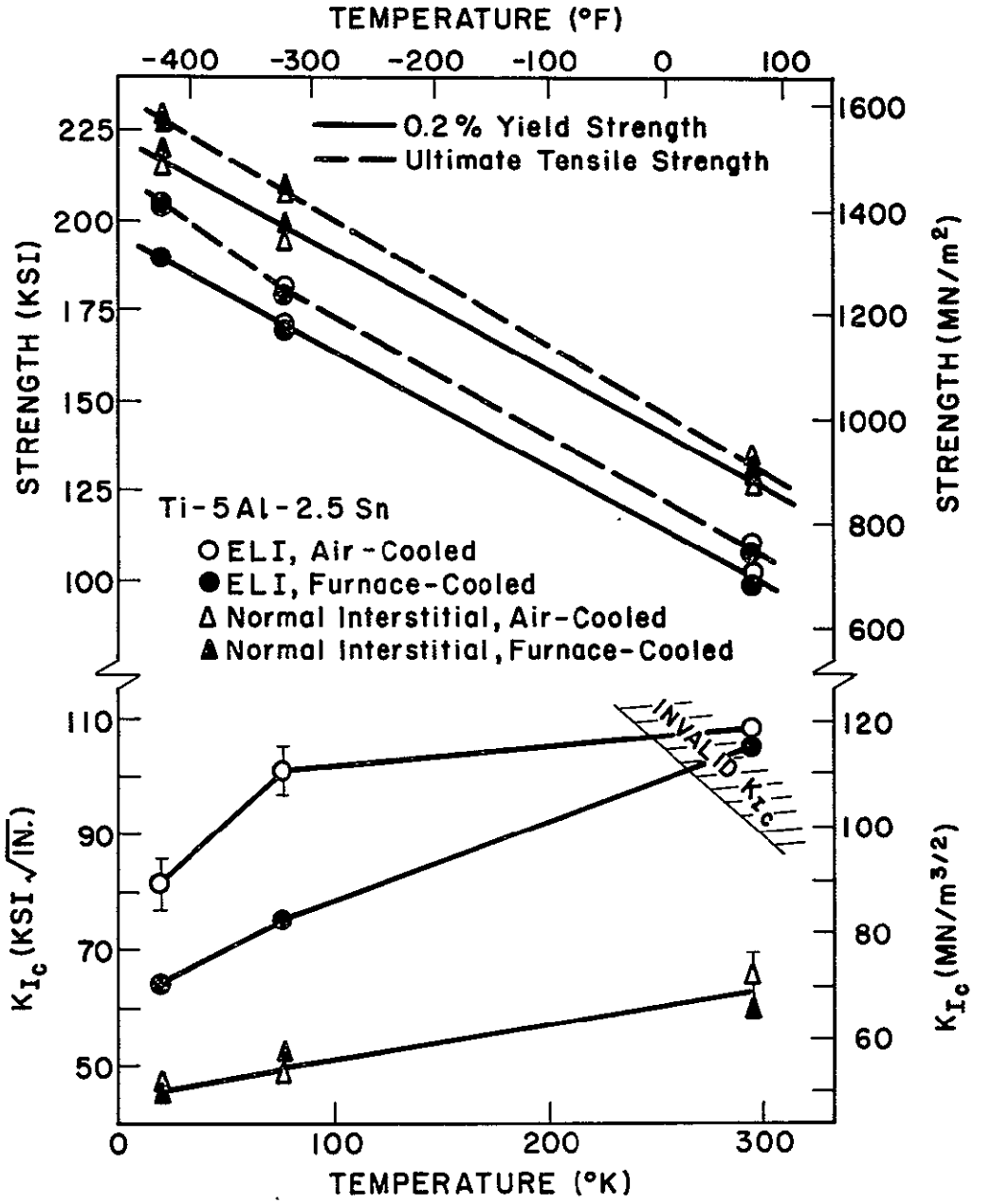

Figure 4. The Variation of Longitudinal Tensile Properties and LT Fracture Toughness of Ti-5Al-2.5Sn with Test Temperature. The error bars indicate the range of plus and minus one standard deviation.

The ELI alloys are much tougher than those of the normal interstitial alloys. Cooling rate from the annealing temperature has no effect on the toughness of the normal interstitial plates, but the air-cooled ELI alloy has a K_{Ic} about 30 percent greater than the furnace-cooled ELI alloy at 20°K and 77°K. Both the air-cooled and furnace-cooled ELI plates have 295°K fracture toughness results which are invalid because of insufficient crack length and specimen thickness. The test record of the furnace-cooled specimen showed that the maximum load and fast fracture occurred at specimen deflections less than the 5 percent secant deflection. In the air-cooled ELI test record, the maximum load exceeded the 5 percent secant load by 32 percent and fast fracture occurred at a specimen deflection much greater than that of the 5 percent secant. These observations of the test records suggest that at room temperature, the air-cooled ELI plate may be tougher than the furnace-cooled ELI alloy even though these materials have similar K_Q values.

High-strength alloys usually show trends of decreasing K_{Ic} with increasing yield strength so the toughness of different alloys should be compared at similar strength levels. The LT orientation fracture toughness of the Ti-5Al-2.5Sn alloys has been plotted as a function of yield strength in Figure 5. The variation of these properties result from changes in testing temperature. These data are the same as those shown in Figure 4 and the error bars have the same meaning as those in Figure 4. The specimens used have nominal crack lengths and thicknesses of 25 mm (1 inch). The region of invalid data shown in Figure 5 shows where these dimensions are too small to meet the ASTM requirement[7] of $2.5\,(K_Q/\sigma_y)^2$. This figure shows the same trends as those noted previously. At similar strength levels, the ELI alloys are tougher than the normal interstitial alloys. Cooling rate does not greatly affect the toughness of the normal interstitial alloys, but furnace cooling greatly reduces the toughness of ELI plates with respect to the K_{Ic} of the air-cooled ELI material.

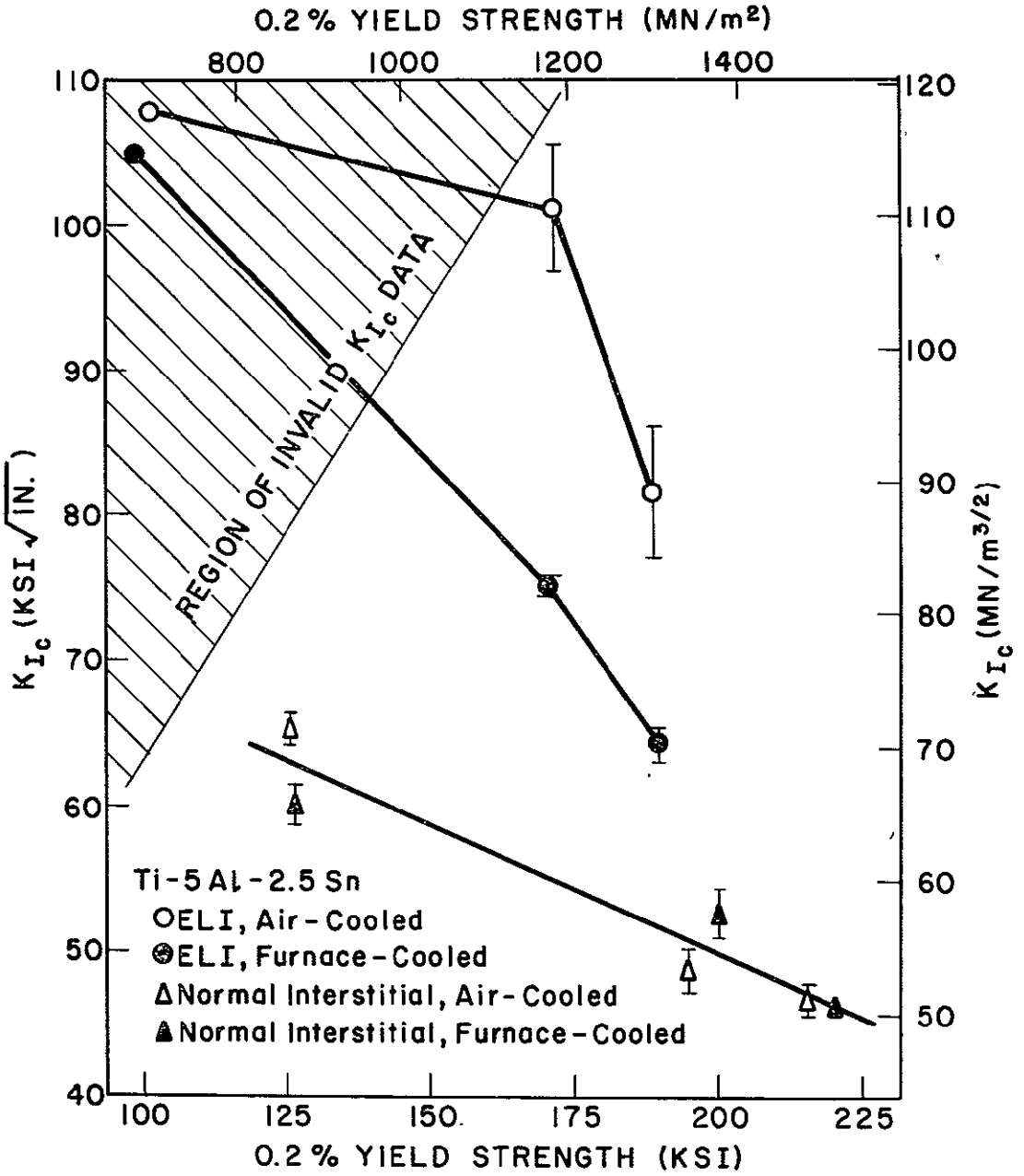

Figure 5. The Variation of LT Fracture Toughness with Longitudinal Tensile Yield Strength of the Ti-5Al-2.5Sn Plates. The variation in strength result from changes in the test temperature. The error bars indicate the range of plus and minus one standard deviation.

The results of the three types of bend specimens used to measure K_{Ic} at 20°K are shown in the form of a bar graph in Figure 6. A schematic of the specimen orientation and relative size is shown in the inset of the figure. The dark regions represent the range of K_{Ic} within one standard deviation of the mean (68 percent confidence limits). All the data shown in Figure 6 meet the ASTM specimen thickness and test record shape requirement,[7] but two sets of data failed to meet criteria associated with the crack length. The crack lengths in the 1x1 LS specimens of the air-cooled ELI alloy were approximately 15 percent less than the 2.5 $(K_Q/\sigma_y)^2$ length required in the standard test method.[7] Technically, these data should be considered as K_Q instead of K_{Ic}; however, there is data in the literature which suggests that the crack length requirement may be too restrictive when the specimen thickness criteria is satisfied. Brown and Srawley[17] noted that the 2.5 $(K_Q/\sigma_y)^2$ crack length requirement may be too strict for steels but they had no data on which to base a more relaxed standard. The data of Nelson and Kaufman[18] on aluminum alloys seems to suggest the same thing. In 1970, Jones and Brown[19] studied the influence of crack length and specimen thickness on K_Q in a steel and noted that the variation in K_Q with crack length is quite small if the thickness criteria is satisfied and if the crack length-to-specimen width ratio (a/W) is between 0.45 and 0.55. Both these requirements were satisfied in the air-cooled ELI 1x1 bend specimens in the LS orientation, so the results of those specimens are considered to be representative of K_{Ic}.

The air-cooled normal interstitial alloy 1x1 bend specimens in the LT orientation are also technically invalid because a/W, the crack length (a) to specimen width (W) ratio, just exceeded 0.55. Jones and Brown[19] have shown that the restrictions on the a/W ratio is required in specimens having test records which greatly deviate from a linear behavior prior to fast fracture. In this type of test record, the load used to calculate K_Q is

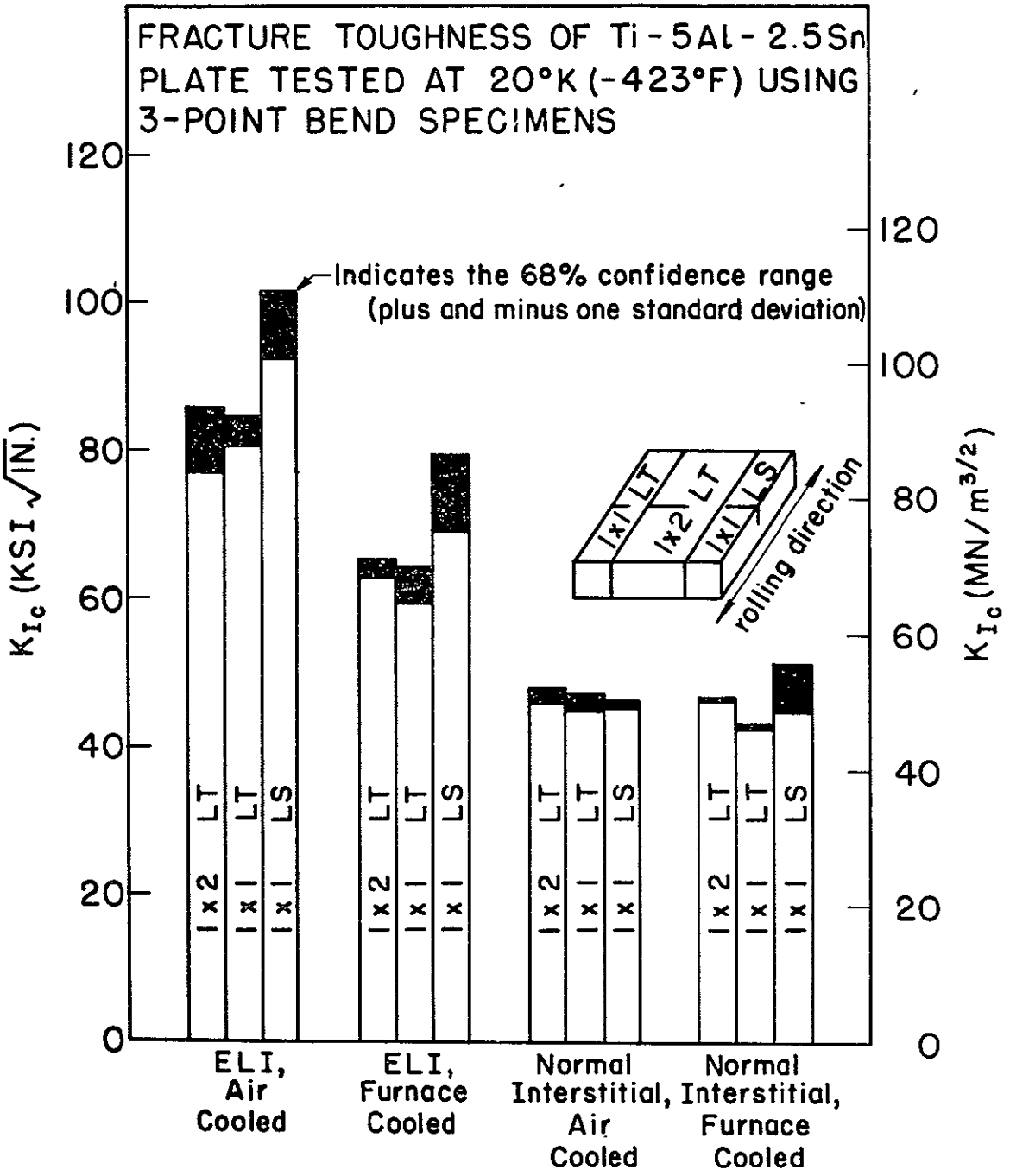

Figure 6. Fracture Toughness of the Ti-5Al-2.5Sn Plates Determined at 20°K using 3-Point Bend Specimens with LS and LT Orientations.

at the intersection of the load-displacement trace and the 5 percent secant line. In a standard specimen with a/W of 0.5, the 5 percent secant corresponds to 2 percent crack growth assuming linear elastic behavior. As a/W changes, the compliance of the specimen also changes and the 5 percent secant line will correspond to a different percentage of crack growth. This criteria is not of importance in the 1x1 LT specimens from the air-cooled normal interstitial Ti-5Al-2.5Sn plate because the maximum load and fast fracture occurred at specimen deflections less than the 5 percent secant line. Jones and Brown[19] reported that in this type of test record, a/W should have little effect on K_Q. Thus, all the data shown in Figure 6 are considered to be valid.

Figure 6 shows that the 1x1 and 1x2 LT orientation bend specimens measure the same K_{Ic} values in a given alloy. Jones and Brown[19] have shown the same effect in steels. This means that the 1x1 bend specimens can be used to evaluate the LS orientation K_{Ic} for these Ti-5Al-2.5Sn plates. Figure 6 shows that the toughness of the two normal interstitial plates are identical in the LT and LS orientations; however, the LS K_{Ic} of both ELI plates is approximately 20 percent greater than the K_{Ic} for specimens with LT orientations.

The tensile flow curves of the Ti-5Al-2.5Sn alloys are shown in Figure 7. The circles represent experimental datum points from multiple specimens and the solid curve is the result of the least squares regression empirical flow curves of the form given in Equation (4). Each empirical flow curve is terminated at the average fracture strain which is indicated by an "X". Many datum points determined from the load-elongation test record are not shown in Figure 7 but were used in the regression analysis. These data were at strains up to about 0.1 for the 295°K and 77°K flow curves, but only up to strains of approximately 0.01 for the 20°K flow

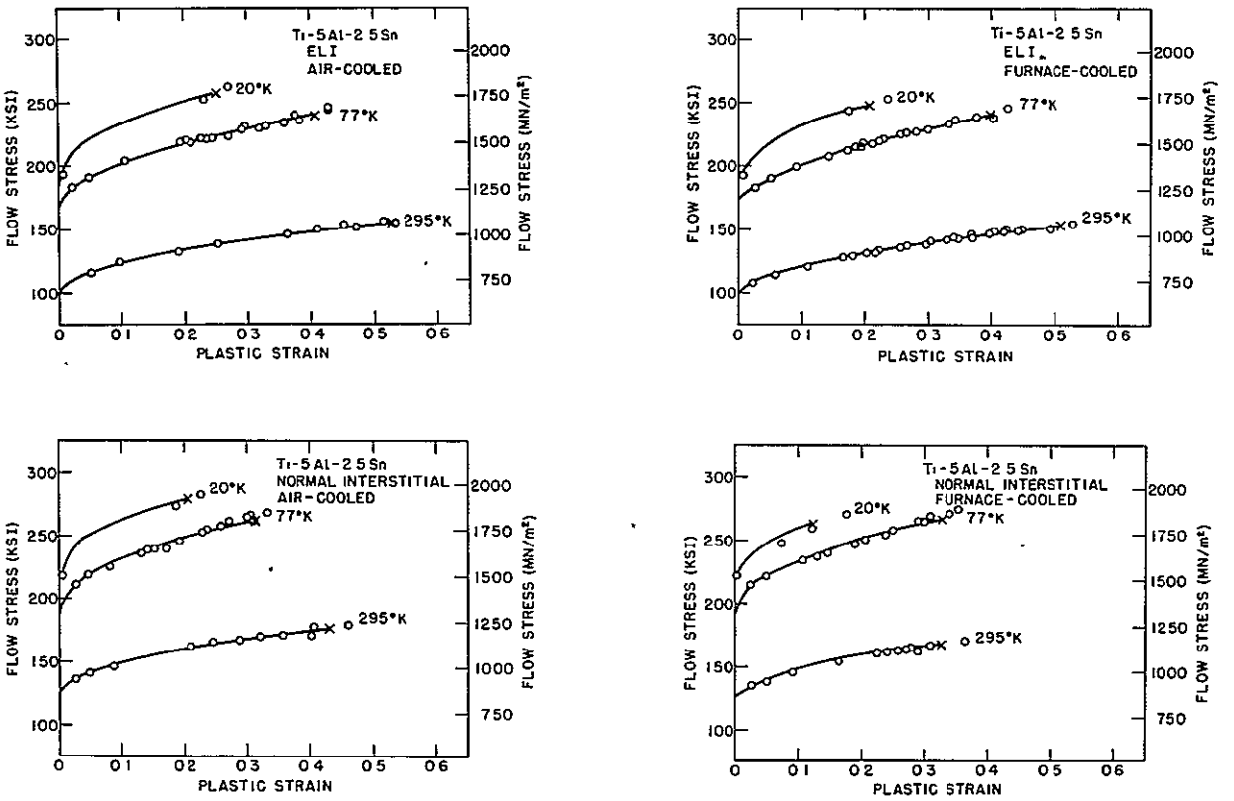

Figure 7. Longitudinal Tensile Flow Curves of the Ti-5Al-2.5Sn Plates. The solid lines are the result of the regression analysis. The "X" represents the average fracture strain.

curves. The constants σ_o, A, and m from the empirical flow curves are listed in Table IV. Also given in the table is the statistical significance which was calculated using a paired t test. This test compared the experimental flow stress with that calculated from the empirical flow curve at the given plastic strain. The significance can be interpreted as the probability that the experimental flow stress data and the empirical flow curve belong to the same population. The lowest significance is 92.9 percent so the fit of the data is excellent.

Caution must be observed when interpreting the 20°K flow curves because no data were obtained between strains of about 0.01 and the fracture strains which are all greater than 0.1. At strains greater than 0.1, the tensile tests at 20°K also exhibited a serrated yielding behavior where the stress-strain curve has sudden load drops. Further crosshead motion after a load drop results in slow increases in load to a level greater than the previous maximum load and then the load drops again. This type of behavior is observed in many alloys at cryogenic temperatures and may be due to adiabatic deformation.[20] Basinski[21] has shown that at cryogenic temperatures, plastic deformation can cause relatively large but localized increases in specimen temperature due to the heat generated during plastic deformation and the extremely small heat capacities at low temperatures. The adiabatic heating results in lower flow stresses because of the rapid reduction in strength level with increasing temperature. Plastic deformation causes local heating which results in lower flow stresses and repetition of this behavior causes serrations of the load-extension record of tensile tests. Kula and De Sisto[20] have observed serrated yielding for unalloyed titanium at 4°K. Carman and Katlin[22] have observed the same behavior in a Ti-5Al-2.5Sn alloy at 20°K. In the Ti-5Al-2.5Sn alloys investigated here, the maximum load in the specimens tested at 20°K occurs at the fracture load. In the 20°K specimens,

TABLE IV

Flow Curves of Ti-5Al-2.5Sn Plate Fit to the Form $\sigma = \sigma_o + A\epsilon^m$

Alloy	Test Temperature °K (°F)	σ_o (ksi) (a)	A (ksi) (a)	m	Level of Significance (%) (b)
Ti-5Al-2.5Sn	295 (72)	98.0	77.5	0.50	93.7
ELI	77 (-320)	166.3	115.8	0.52	98.3
Air-Cooled	20 (-423)	172.5	135.6	0.35	98.8
Ti-5Al-2.5Sn	295 (72)	96.4	81.5	0.54	93.0
ELI	77 (-320)	165.9	121.3	0.55	>99.9
Furnace-Cooled	20 (-423)	171.2	132.4	0.35	97.1
Ti-5Al-2.5Sn	295 (72)	120.5	82.9	0.47	96.8
Normal Interstitial	77 (-320)	180.3	129.2	0.40	96.4
Air-Cooled	20 (-423)	185.8	140.1	0.26	94.7
Ti-5Al-2.5Sn	295 (72)	123.4	81.2	0.55	92.9
Normal Interstitial	77 (-320)	189.9	127.5	0.46	93.2
Furnace-Cooled	20 (-423)	185.8	116.7	0.21	97.2

(a) 1 ksi = 6.9 MN/m^2

(b) Determined using a t - test on paired data

several necked regions could be observed away from the fracture surface of broken tensile specimens. Kula and De Sisto[20] have reported that multiple necking is a common characteristic of adiabatic deformation and is due to the localization of the heating. Serrated yielding and multiple necking were not observed in specimens tested at 77°K or 295°K. These observations are consistent with those of Kula and De Sisto[20] on unalloyed titanium.

Care must be observed when making comparisons between the σ_o values in Table IV because the load extension curves at 20°K were determined using strain gages with a strain resolution of 0.00002 while at the higher test temperatures, the test record had a strain resolution of 0.0001. At these temperatures, the resolution of the LVDT was not fully used so that the load-elongation curves could be monitored up to the maximum load. The higher strain resolution at 20°K will increase the ability to observe small deviations from linear elastic behavior and thus decrease the apparent elastic limit σ_o.

It is interesting to note that the exponent on strain m listed in Table IV for 295°K and 77°K are close to 0.5. This was the value assumed in previous studies on titanium-oxygen[23] and titanium-aluminum alloys.[24]

The rate of strain hardening was calculated by differentiation of the empirical flow curve given in Equation (4) with respect to strain.

$$\frac{\partial \sigma}{\partial \varepsilon} = m A \dot{\varepsilon}^{m-1} \tag{5}$$

At a given strain, work hardening is dependent on m and A and independent of σ_o. Figure 8 shows the work-hardening rate for the Ti-5Al-2.5Sn alloys at 77°K and 295°K as a function of plastic strain. The 20°K data were not included because of the lack of data at intermediate strains and uncertainties caused by serrated yielding. The work-hardening rate is greater at 77°K

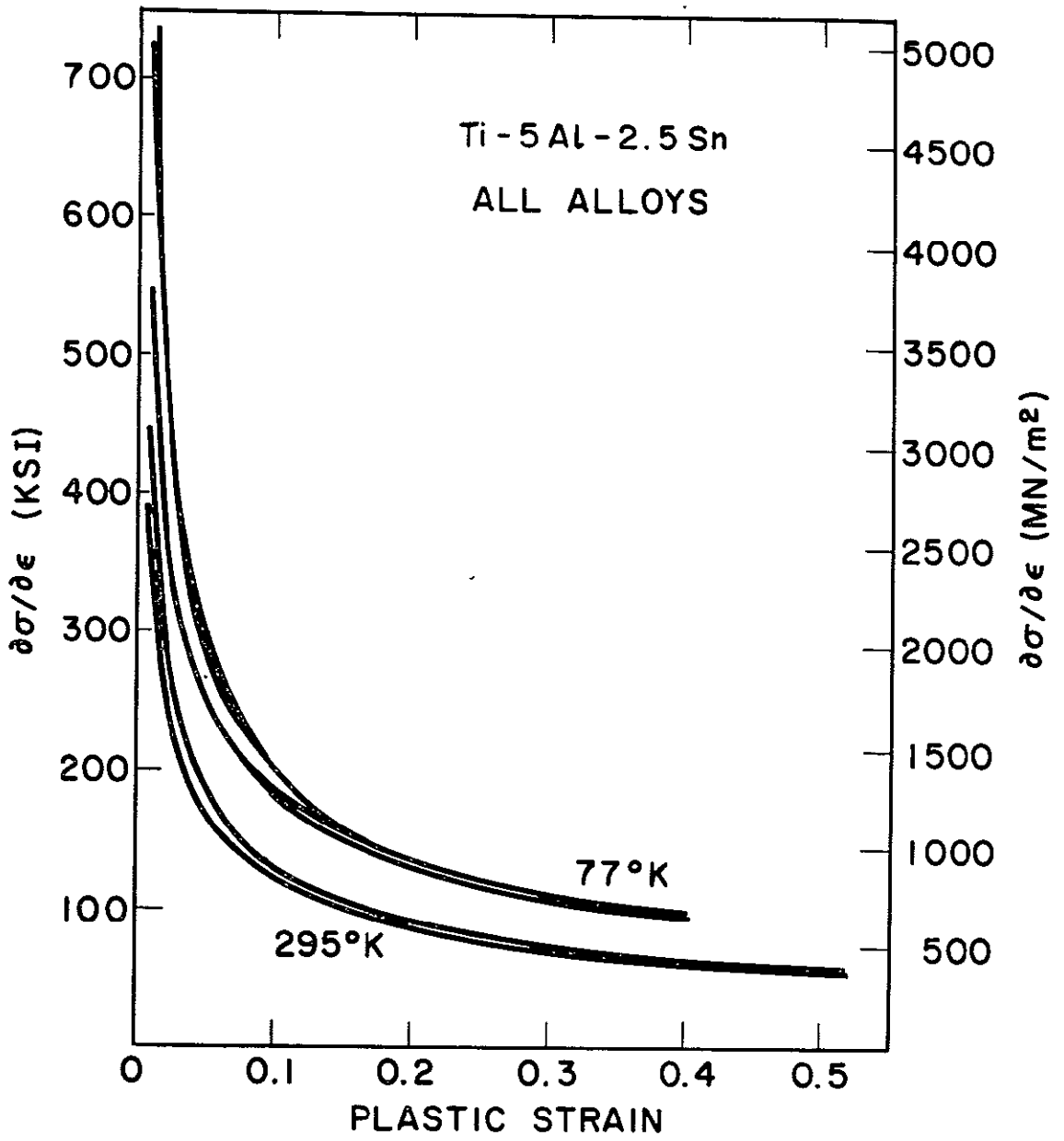

Figure 8. Variation of the Work-Hardening Rate ($\partial\sigma/\partial\epsilon$) of the Ti-5Al-2.5Sn Alloys with Plastic Strain and Test Temperature.

that at 295°K. The strain hardening behavior seems to be independent of alloy purity and cooling rate and seems to be only a function of testing temperature. The work hardening at 20°K was similar to that at 77°K, but that result is questionable because of the uncertainty of the 20°K flow curves. The difference in the flow curves between the ELI and normal interstitial alloys result largely from increasing the apparent elastic limit (σ_o) with decreasing alloy purity. Similar observations have been made by Conrad, Okasaki, Gadgil, and Jon[23] in unalloyed titanium.

The tensile fracture strain data given in Table III has been analyzed using a t test to determine if the cooling rate significantly affects tensile ductility. For a given alloy purity and test temperature, the probability that tensile ductility varies with cooling rate was always less than 80 percent. Thus, while fracture strain is not significantly affected by cooling rate, the fracture toughness in some cases can be different by 30 percent. This result points out the danger of trying to qualitatively assess the toughness of titanium alloys with tensile ductility data.

The Young's modulus of the Ti-5Al-2.5Sn alloys was determined from multiple tensile specimens at 20°K and from single determinations at room temperature using ultrasonic techniques. The ultrasonic data was determined at the Rockwell Science Center in Thousand Oaks, California. In unalloyed titanium, the Young's modulus perpendicular to the basal plane is 45 percent greater than the modulus in the basal plane.[25] Thus, crystallographic texture can have a great influence on the elastic properties. For that reason, the raw data used to generate the texture pole figures were used to calculate the Young's modulus as function orientation in the Ti-5Al-2.5Sn plates. The computer program used to calculate the modulus is that described by Olsen and Moreen[26] and assumes the single crystal elastic constants are those determined for unalloyed titanium.

Table V lists the longitudinal Young's modulus determined at 20°K and 295°K along with the longitudinal modulus predicted by the computer program from the measured textures. The modulus of the normal interstitial alloys is clearly greater than the modulus of the ELI alloys. This effect was predicted by the computer analysis which strongly suggested that the variation in modulus is due to crystallographic texture. This can be qualitatively predicted from the pole figures and knowing that Young's modulus perpendicular to the basal plane is 45 percent greater than that in the basal plane. The normal interstitial alloys have a β-processed texture with basal planes normal to the longitudinal direction while the α-annealing texture in the ELI alloys causes the longitudinal stress to act parallel to the basal planes. The difference between the experimental and predicted modulus at 295°K results from the influence of aluminum and tin on the modulus. It is known that aluminum increases the Young's modulus of α titanium,[27] but it is not clear that all the single crystal elastic constants would change in proportional fashion. The average ratio of the experimental modulus to those predicted is 1.11 with a standard deviation of 0.01. This low standard deviation suggests that the computer predictions are a good qualitative tool for analyzing the variation of Young's modulus in alloyed α-titanium.

Figure 9 shows the predicted Young's modulus for the Ti-5Al-2.5Sn alloys at 295°K as a function of orientation in the plane of the plates. The normal interstitial alloys show very little variation but the ELI alloys become stiffer as the orientation is rotated from the longitudinal to transverse directions. Once again this effect can be qualitatively predicted from the pole figure. In the ELI plates, there is an absence of basal plane perpendicular to the longitudinal direction, but there are some basal planes split toward the transverse directions. Increasing the number of grains with basal planes perpendicular to the tensile axis would tend to increase

TABLE V

Longitudinal Young's Modulus (E) of Ti-5Al-2.5Sn Alloys

	E at 20°K[a] (10^6 psi)[d]	E at 295°K[b] (10^6 psi)	Predicted[c] E at 295°K (10^6 psi)
ELI, Air-Cooled	18.1 ± 0.1	16.8	15.3
ELI, Furnace-Cooled	18.4 ± 0.1	16.9	15.2
Normal Interstitial, Air-Cooled	19.2 ± 0.1	18.0	16.1
Normal Interstitial, Furnace-Cooled	19.4 ± 0.1	18.0	16.1

(a) Determined with tensile specimens. Error limits represent range of 68 percent confidence limits.

(b) Determined with ultrasonic techniques.

(c) Predicted by computer program of Olsen and Moreen[26]

(d) 10^6 psi = 6900 MN/m^2

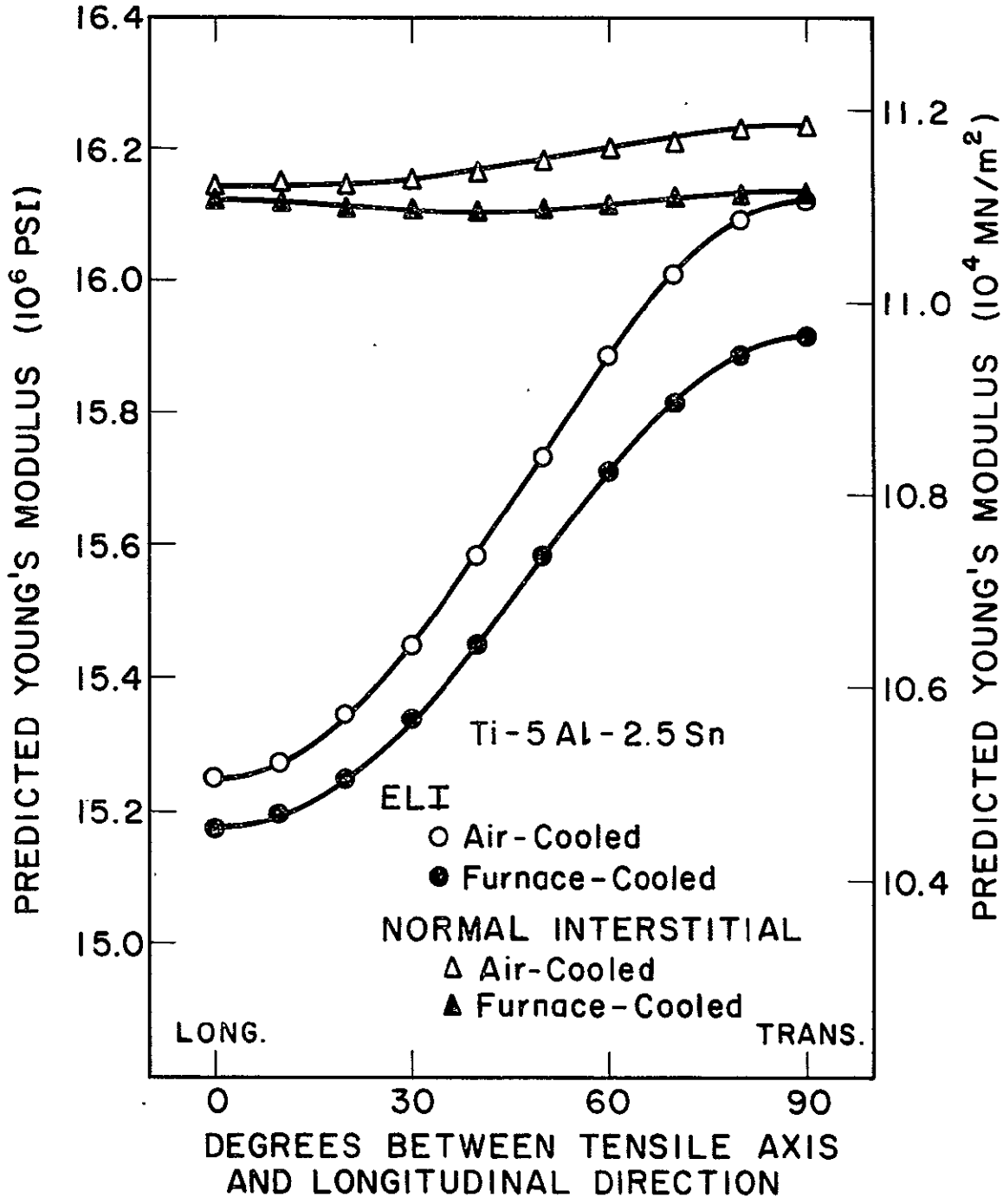

Figure 9. Predicted Room Temperature Young's Modulus of the Ti-5Al-2.5Sn Plates as a Function of Orientation.

the modulus. In the normal interstitial plates, there are no large effects of orientation because basal planes are perpendicular to both the longitudinal and transverse directions. Only the ELI alloys have predicted changes in Young's modulus and observed changes in K_{Ic} with specimen orientation. This tends to suggest that texture may also affect K_{Ic}.

The investigation of Shannon and Brown[4] on Ti-5Al-2.5Sn alloys correctly assessed the influence of interstitial level and cooling rate on toughness using the notched strength of sharply notched sheet tensile specimen. This type of specimen may provide a good measure of toughness for screening tests and quality control of Ti-5Al-2.5Sn. Kaufman and Holt[28] have shown that various measurements made on notch sheet specimens correlate well with K_{Ic} in aluminum alloys.

DISCUSSION

Evaluation of the mechanical properties of the Ti-5Al-2.5Sn plates showed that decreases in temperature result in higher strength levels and lower fracture toughness. The ELI plates were tougher than the normal interstitial level materials. Furnace-cooling from the annealing treatment resulted in ordering of the α matrix and reductions in K_{Ic} of the ELI plate with respect to that of the air-cooled material. Variations in cooling rate did not affect the toughness of the normal interstitial material. In the ELI plate, the LS orientation had a higher K_{Ic} than the LT orientation. No significant changes in toughness were observed with specimen orientation in the normal interstitial plates.

A detailed investigation of the 77°K fracture mechanism in these plates has explained why some of these variations occur and has led to suggestions on other trends.[11] The fracture mechanism is dimpled rupture where approximately half the fracture surface is covered by elongated

dimples. Figure 10 shows a scanning electron microscope fractograph of a furnace-cooled ELI fracture toughness specimen which was tested at 77°K. The region shown in Figure 10 is just ahead of the fatigue precrack and the direction of crack propagation is from left to right. The letter A indicates an elongated dimple and B is in a region of equiaxed dimples.

The equiaxed dimples formed from cigar-shaped voids. These voids nucleated at the intersection of intense localized shear deformation (slip bands or deformation twins) with grain boundaries or deformation twin boundaries. Figure 11 shows examples of slip band - twin boundary offsets and void nucleation are shown in the optical micrograph of a region 45 μm below the fracture surface of an air-cooled ELI tensile tested at 77°K. Two sets of parallel etched bands intersect with twin and grain boundaries resulting in offsets. The planar nature of dislocation arrays in these alloys and the observation that the bands terminate at grain boundaries suggest that slip bands are sometimes etched. Two voids indicated by arrows were observed at offsets in the primary twin boundary. No void exists at the offset labeled A showing that the voids nucleate after offsets have formed.

Voids were also observed to nucleate by decohesion of the interface between the iron-stabilized β phase. This was observed extensively in the normal interstitial alloys but was seldom seen in the ELI plates. This most likely is due to the smaller size of the β phase in the low iron ELI alloys.[29,30] It is interesting to note that the iron content of the ELI alloys (0.15 percent) is very close to 0.20 percent iron level where Broadwell and Wood[2] observed sudden decreases in notched strength-to-yield strength ratios of Ti-5Al-2.5Sn alloys.

Extensive fractographic and metallographic examinations showed that the fracture process by elongated dimples in Ti-5Al-2.5Sn is that

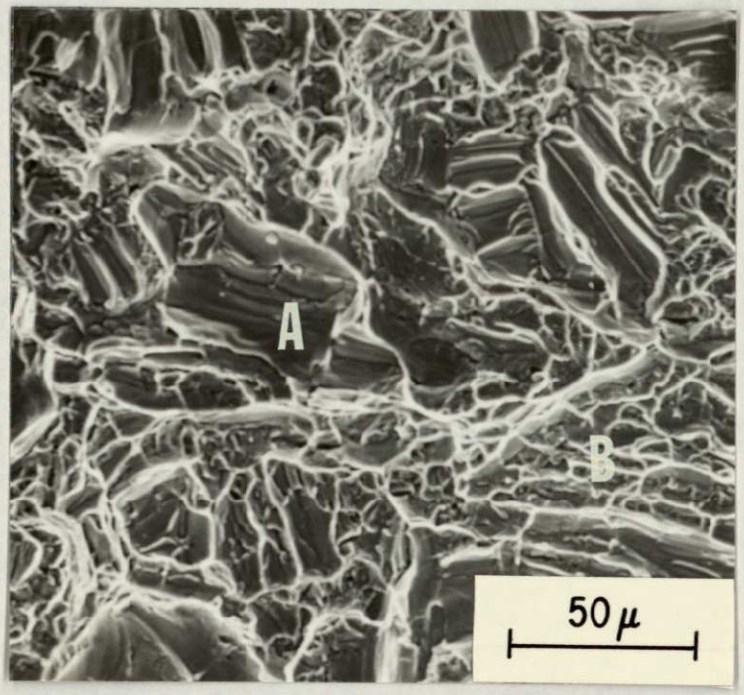

Figure 10. SEM Fractograph of a Furnace-Cooled ELI Ti-5Al-2.5Sn Fracture Toughness Specimen Tested at 77°K. The direction of crack propagation is from left to right.

C-2

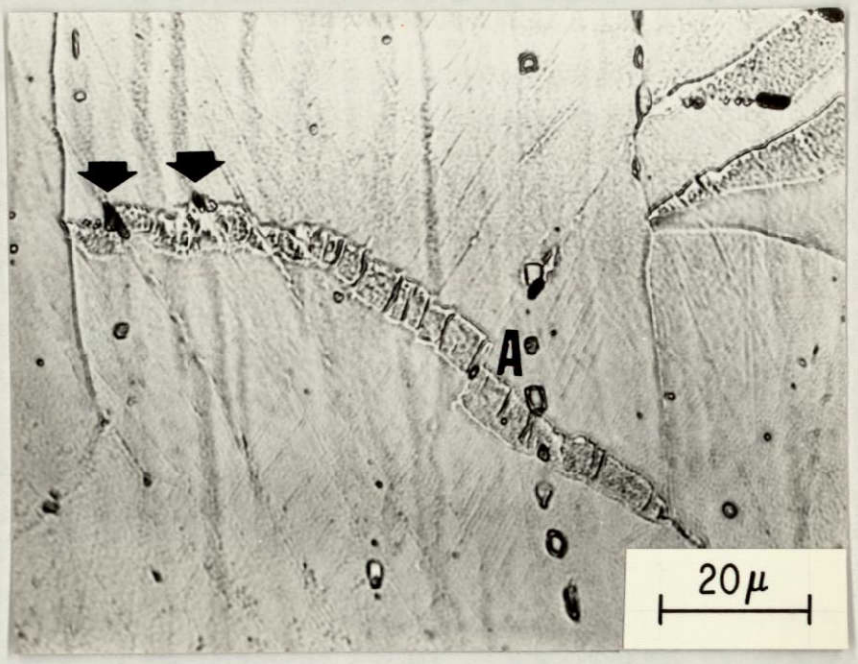

Figure 11. Offsets and Void Nucleation Along Primary Twin Boundaries in an Optical Micrograph of a Sectioned Air-Cooled ELI Ti-5Al-2.5Sn Tensile Specimen Strained to 0.348 at 77°K. The arrows point to voids along the primary twin boundary at offsets. The letter "A" indicates an offset without void nucleation. The tensile axis is vertical.

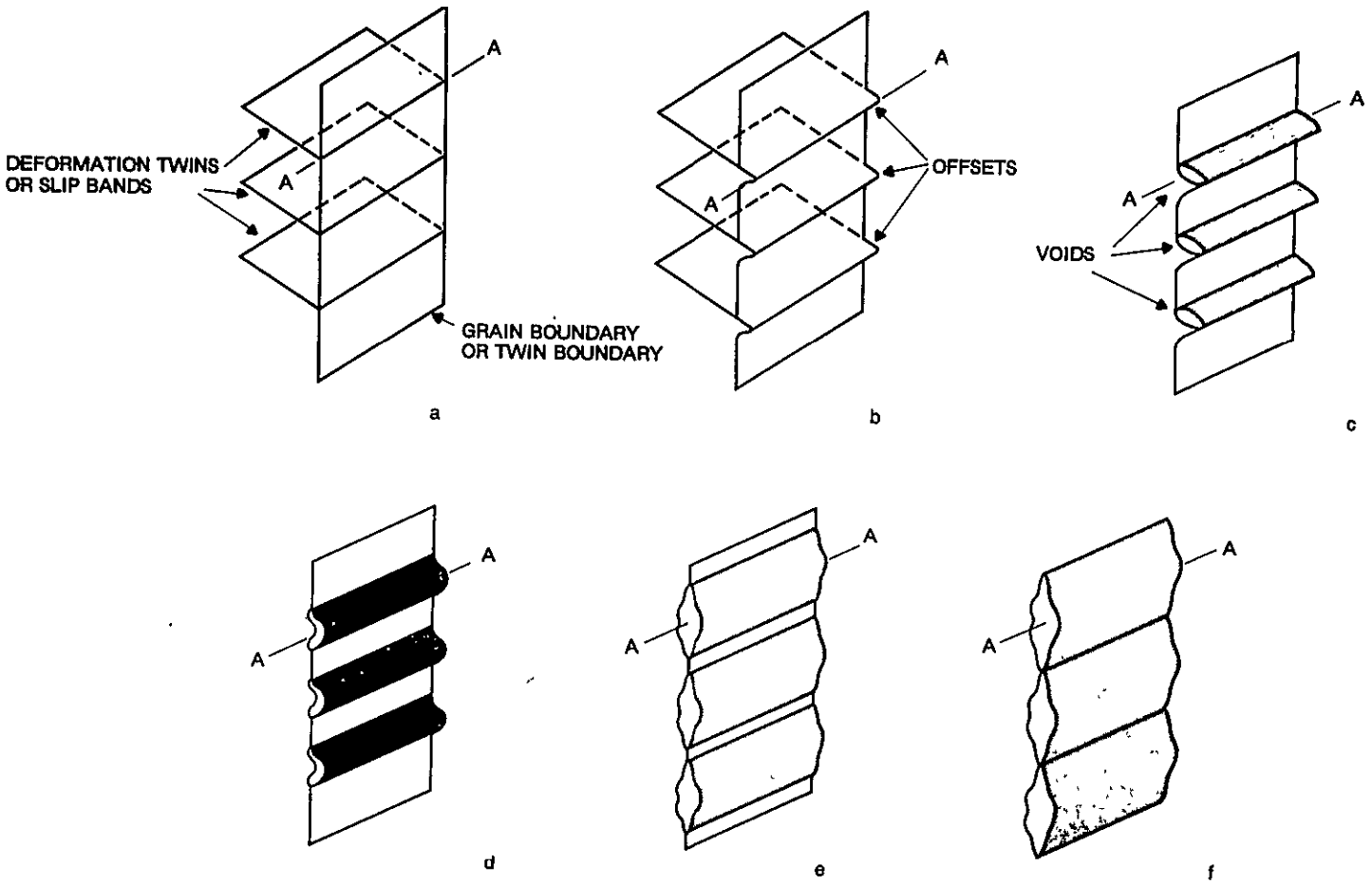

Figure 12. Schematic of the Sequence of Events During Fracture by Elongated Dimples.

and fracture processes explain qualitatively why these alloys have variations in toughness.

To examine the influence of texture and specimen orientation on K_{Ic}, a computer program similar to the one described by Thornburg[31] was written to describe the resolved shear stress on a given slip or twin system as a function of the position of the c-axis on a stereographic projection for an arbitrarily imposed stress state. The deformation systems included the four slip system (prism, basal, pyramidal, and c+a $(10\bar{1}1)$) and five twin systems ($(10\bar{1}2)$, $(11\bar{2}1)$, $(11\bar{2}2)$, $(11\bar{2}3)$, and $(11\bar{2}4)$) known to operate at cryogenic temperatures in α titanium.[32]

It will be assumed that the criteria for deformation by slip will be the critical resolved shear stress. The index used to evaluate the operation of a given slip system is the resolved shear stress divided by the critical resolved shear stress for that particular slip system. The critical resolved shear stresses determined by Paton, Baggerly, and Williams[33] for titanium - 6.6 percent aluminum crystals at 77°K were used for the normalization. The index used for the activation of twin systems will be a resolved shear stress criteria. There is no established critical resolved shear stress for twinning; however in most cases, the twin system with the highest resolved shear stress is the first system to operate.[34] Reed-Hill[35] has shown that in polycrystalline zirconium, the variation in number of twins for several twin systems is very similar in shape to the variation in the resolved shear stress with the angle between the applied stress and c-axis. Thus, the resolved shear stress appears to be an adequate index to determine if a given twin system is operating.

To examine toughness variations between the LS and LT orientation fracture toughness specimens, a stress state typical of that ahead of a crack will be used in the computer program. There are many elasto-plastic

finite element calculations which show the variation of the stresses with position and work-hardening characteristics.[36, 37] Levy and co-workers[38] have analyzed the crack tip stress fields of elastic-perfectly plastic (non work-hardening) material using both slip line field theory and finite element calculations. Those solutions will be used in the resolved shear stress calculations because the ratios between the normal stresses in the work-hardening solutions are similar in many cases to the slip line field solutions. The stresses were normalized so that the maximum stress which is parallel to the applied load is equal to unity. The normalized stresses used to calculate the resolved shear stresses for the LS and LT orientation fracture toughness specimens are given in Table VI. In both cases, the maximum stress acts in the longitudinal direction and is the same so that equivalent levels of K_I are being compared.

The stereographic projections in Figure 13 show the variation in the resolved shear stresses for slip normalized by the critical resolved shear stress for LT and LS orientation fracture toughness specimens. Figure 14 shows the resolved shear stress for twinning for the same stress states. Figure 13 shows that for alloys with an α annealing texture, specimens with an LT orientation will tend to deform by prism and pyramidal slip at a lower K_I level than specimens with an LS orientation. For LS specimens with this texture, the tendency for basal slip is less than that for other a slip modes. For both orientations, $\overrightarrow{c+a}$ slip seems to be fairly unlikely. Figure 14 shows that the resolved shear stress for twinning in plates with an α annealing texture is fairly low except for $(11\bar{2}2)$ twinning. This twinning system is most likely to occur at lower K_I levels in the LS specimen than one with an LT orientation. Void nucleation in the ELI alloys occurs most frequently at the intersection of slip bands with twin boundaries or grain boundaries. It was argued that a reduction in slip band length and a more even distribution of slip would delay void nucleation

TABLE VI

Normalized Stresses used for Calculation of the Resolved Shear Stresses for LS and LT Orientation Fracture Toughness Specimens

Stress Axis	LT Specimen	LS Specimen
Longitudinal	1.000	1.000
Transverse	0.607	0.804
Short-Transverse	0.804	0.607

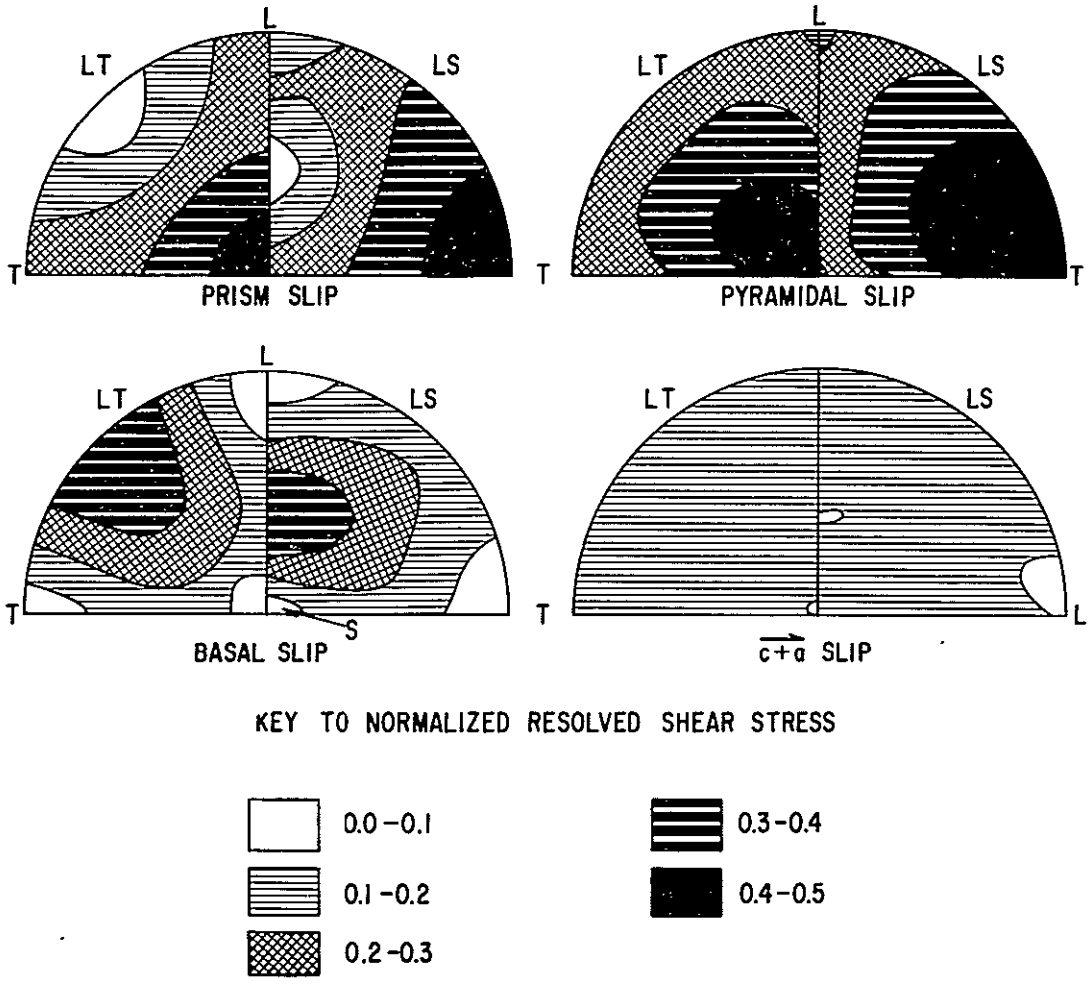

Figure 13. Stereographic Projections Showing the Variation of Normalized Resolved Shear Stress for Slip in LS and LT Orientation Fracture Toughness Specimens. L, T, and S indicate longitudinal, transverse, and short transverse directions, respectively.

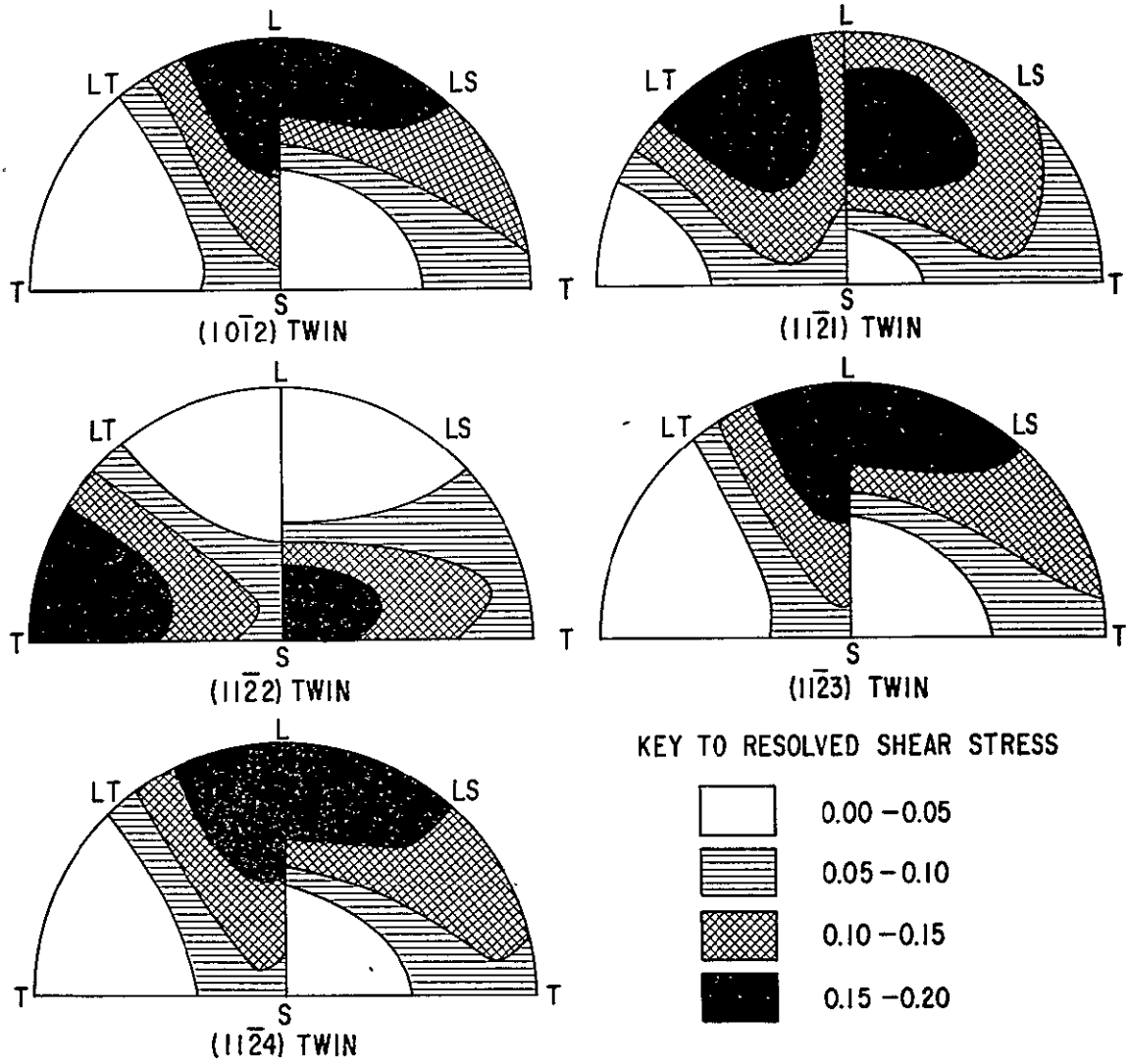

Figure 14. Stereographic Projections Showing the Variation of Resolved Shear Stress for Twinning in LS and LT Orientation Fracture Toughness Specimens. L, T, and S indicate longitudinal, transverse, and short transverse directions, respectively.

to higher strains and in turn improve K_{Ic}.[11] Calculation of the resolved shear for slip for LS and LT fracture toughness specimens suggests that slip will occur at lower K_I levels in LT specimens than LS specimens. Thus, at the same K_I level, there will probably be more dislocations per slip band in the LT specimens. The higher resolved shear stress for twins in the LS specimens suggests that the LS orientation will have a higher twin volume fraction than the LT specimen. A higher twin volume fraction of the $(11\bar{2}2)$ twins will tend to reduce the slip band length. These factors suggest that the LS K_{Ic} value will be higher than that for LT specimens for alloys with an α annealing texture. This prediction is consistent with the K_{Ic} values for the air-cooled and furnace-cooled ELI alloys.

The normal interstitial alloys have a β processed texture. The resolved shear stresses on twin systems shown in Figure 14 suggests that $(10\bar{1}2)$, $(11\bar{2}1)$, $(11\bar{2}3)$, and $(11\bar{2}4)$ twins are equally likely to occur for both LS and LT specimens with a β processed texture. Twins of the $(11\bar{2}2)$ system may also occur for LT specimens. Void nucleation in the normal interstitial alloys occurred most frequently at multiple twin intersections.[11] The resolved shear stress data on the twin system suggests that twinning can occur on many twin systems for fracture toughness specimens with both LS and LT orientations. From this, one would expect that K_{Ic} would be similar for both orientations.

The experimental investigation of the microscopic fracture mechanism, the K_{Ic} data, and the analysis of the texture-deformation maps have led to several suggestions on how to improve the toughness of Ti-5Al-2.5Sn at cryogenic temperature. K_{Ic} can be increased by having the lowest possible interstitial level, cooling rapidly from the annealing temperature to avoid ordering, and reducing the iron content to 0.15 percent. It was suggested that reduction in α grain size and texture - stress

state combinations which suppress multiple twinning would also improve K_{Ic}.

CONCLUSIONS

Evaluation of the mechanical properties of Ti-5Al-2.5Sn plate material has been performed over the temperature range from 20°K to 295°K. Decreases in test temperature and higher interstitial level resulted in increased yield strength and decreased fracture toughness. Variation in cooling rate from the annealing temperature had no influence on strength and tensile ductility. The changes in cooling rate did not affect K_{Ic} of the normal interstitial plates but K_{Ic} of the air-cooled ELI plate was 30 percent greater than that of the furnace-cooled ELI plate. The combination of specimen orientation and crystallographic texture cause variations in Young's modulus and K_{Ic}. LS orientation fracture toughness was 20 percent greater than LT K_{Ic} in the ELI plates but no variations in K_{Ic} were observed with specimen orientation in the normal interstitial alloys.

Fractography and metallographic sectioning were used to investigate the fracture mechanism. It was shown that the fracture mechanism is dimpled rupture where voids nucleate at the intersection of intense localized shear bands with crystallographic boundaries. Increasing interstitial content and ordering caused by furnace-cooling from the annealing temperature cause the slip band structure to become coarser. The higher strain per slip band increases the rate of void nucleation and as a result decreases fracture toughness. An analysis at the tip of a crack in these textured plates was used to explain the variations in toughness with specimen orientation. It was also suggested that reductions in α grain size would improve K_{Ic}.

ACKNOWLEDGMENTS

This work was performed under National Aeronautics and Space Administration Grant NGR-39-087-047. The authors would like to thank W. F. Brown, Jr., W. S. Pierce, and W. D. Klopp of that organization for their helpful support and comments. We also wish to acknowledge the valued assistance of Mrs. Jean Ballew in the preparation of this manuscript.

REFERENCES

1. J. L. Christian, A. Hurlich, J. E. Chafey, and J. F. Watson, Proc. ASTM, 63, 1963, p. 578.
2. R. G. Broadwell and R. A. Wood, Materials Research and Standards, 4, 1964, p. 549.
3. H. W. Worner, J. Inst. of Metals, 79, 1951, p. 173.
4. J. L. Shannon, Jr. and W. F. Brown, Jr., Proc. ASTM, 63, 1963, p. 809.
5. M. J. Blackburn, Trans. AIME, 239, 1967, p. 1200.
6. T. K. G. Namboodhiri, C. J. McMahon, Jr., and H. Herman, Met. Trans., 4, 1973, p. 1323.
7. "Standard Method of Test for Plane-Strain Fracture Toughness of Metallic Materials," ASTM Designation E399-74.
8. R. E. Curtis, R. R. Boyer, and J. C. Williams, Trans. ASM, 62, 1969, p. 457.
9. P. P. Dessau and C. L. Harris, "Premium Quality 5Al-2.5Sn ELI Titanium Production, Final Report," NASA-CR-132227, Aerojet Nuclear Systems Co., Azusa, California, May 1972.
10. W. G. Reuter, "Fracture Toughness of Ti-5Al-2.5Sn ELI Forgings at -423°F," Summary Report, Aerojet-General Corporation, Sacramento, California, September 9, 1970.
11. R. H. Van Stone, J. R. Low, Jr., and J. L. Shannon, Jr., "The Fracture Mechanism of Ti-5Al-2.5Sn at Cryogenic Temperatures," to be published.
12. J. L. Shannon, Jr., R. T. Bubsey, and W. S. Pierce, "Plane Strain Fracture Toughness Assessment of Thick-Walled Liquid Hydrogen Transfer Pipe made of Welded Centrifugally-Cast 21-6-9 Stainless Steel," to be published.
13. J. L. Shannon, Jr. and W. S. Pierce, "An LVDT Type Displacement Gage for Plane-Strain Fracture Toughness Tests in Liquid Hydrogen, to be published.
14. P. W. Bridgman, Studies in Large Plastic Flow and Fracture, McGraw-Hill, New York, 1952.

15. S. N. Monterio and R. E. Reed-Hill, Met. Trans., 4, 1973, p. 1011.

16. J. G. Kaufman and F. J. Cordier, Alcoa Laboratories, unpublished research.

17. W. F. Brown, Jr., and J. E. Srawley, ASTM STP 410, 1966.

18. F. G. Nelson and J. G. Kaufman, "The Effect of Specimen Size on the Results of Plane-Strain Fracture Toughness Tests," presented at the Fourth National Symposium on Fracture Mechanics, Pittsburgh, Pennsylvania, August 18, 1970.

19. M. H. Jones and W. F. Brown, Jr., ASTM STP 463, 1970, p. 63.

20. E. Kula and T. DeSisto, ASTM STP 387, 1966, p. 3.

21. Z. S. Basinski, Proc. Roy. Soc., London, A240, 1957, p. 229.

22. C. M. Carman and J. M. Katlin, ASTM STP 432, 1968, p. 124.

23. H. Conrad, K. Okasaki, V. Gadgil, and M. Jon, Electron Microscopy and Structure of Materials, University of California Press, Berkeley, 1972, p. 438.

24. D. J. Truax and C. J. McMahon, Jr., Mat. Sci. Eng., 13, 1974, p. 125.

25. Frank Larson and Anthone Zarkades, "Properties of Textured Titanium Alloys," Metals and Ceramics Information Center, Report MCIC-74-20, Battelle Columbus Laboratories, Columbus, Ohio, June 1974.

26. R. H. Olsen and H. A. Moreen, Met. Trans., 4, 1973, p. 701

27. H. R. Ogden, D. J. Maykuth, W. L. Finlay, and R. I. Jaffee, Trans. AIME, 197, 1953, p. 267.

28. J. G. Kaufman and Marshall Holt, "Fracture Characteristics of Aluminum Alloys," Aluminum Company of America, ARL Technical Paper No. 18, 1965.

29. R. H. Van Stone, R. H. Merchant, and J. R. Low, Jr., ASTM STP 556, 1974, p. 93.

30. T. B. Cox and J. R. Low, Jr., Met. Trans., 5, 1974, p. 1457.

31. D. A. Thornburg, "Cold-Rolling Texture Development in Titanium and Titanium-Aluminum Alloys," Ph. D. Thesis, Department of Metallurgy and Materials Science, Carnegie-Mellon University, 1972.

32. N. E. Paton, J. C. Williams, and G. P. Rauscher, Titanium Science and Technology, Plenum Press, New York, 1973, p. 1049.

33. N. E. Paton, R. G. Baggerly, and J. C. Williams, "Deformation and Solid Solution Strengthening of Titanium Aluminum Single Crystals," Report SC 526.7FR, Rockwell International Science Center, January 20, 1976.

34. S. Mahajan and D. F. Williams, Met. Rev., 18, 1973, p. 43.

35. R. E. Reed-Hill, Deformation Twinning, Gordon and Breach, New York, 1964, p. 295.

36. C. F. Shih, ASTM STP 590, 1974, p. 187.

37. J. R. Rice and C. F. Rosengren, J. Mech. Phy. Solids, 16, 1968, p. 1.

38. N. Levy, P. V. Marcal, W. J. Ostergren, and J. R. Rice, Int. J. Fracture Mech., 7, 1971, p. 143.